의학석사 학위논문

Quantification of Fat Fraction in the Liver Using Dual Energy Computed Tomography and Multi-material Decomposition

이중에너지 전산화 단층촬영과 다물질분해 방법을 이용한 간 내 지방분율의 정량화 연구

2014 년 2 월

서울대학교 대학원

의학과 영상의학 전공

허 보 윤

↑
2cm
↓

이중에너지 전산화 단층촬영과 다물질분해
방법을 이용한 간 내 지방분율의 정량화 연구

↑
2.5cm
↓

2014년

↑
4cm
↓

↑
3cm
↓

허보윤

↑
2cm
↓

이중에너지 전산화 단층촬영과 다물질분해 방법을 이용한 간 내 지방분율의 정량화 연구

지도 교수 이 정 민

이 논문을 의학석사 학위논문으로 제출함
2013년 10월

서울대학교 대학원
의학과 영상의학 전공
허 보 윤

허보윤의 의학석사 학위논문을 인준함
2013년 12월

위 원 장 한 준 구 (인)
부위원장 이 정 민 (인)
위 원 이 광 웅 (인)

Quantification of Fat Fraction in the Liver Using Dual Energy Computed Tomography and Multi-material Decomposition

by
Bo Yun Hur

A thesis submitted to the Department of Radiology in partial fulfillment of the requirement of the Degree of Master of Philosophy in Radiology at Seoul National University College of Medicine

Febrary 2014

Approved by Thesis Committee:

Professor _____Chairman
Professor _____Vice chairman
Professor _____

ABSTRACT

Purpose: To evaluate the feasibility and accuracy of dual-energy CT (DECT) using multi-material decomposition (MMD) for quantification of the hepatic fat fraction (HFF) and to evaluate the diagnostic performance compared with the precontrast CT number using the histologic examination as the reference standard and MR fat quantification as the technical standard.

Methods: This study was approved by our Institutional Animal Care and Use Committee and our Institutional Review Board. In this animal study, various degrees of fatty liver were induced in 16 rabbits in four groups, by feeding them a high-fat, high-cholesterol diet during 0, two, four, and six weeks, respectively. After 6 weeks, precontrast, single-energy CT and multiphasic DECT were performed and HFF maps were obtained from the multiphasic DECT using MMD. Chemical shift MRI for obtaining the fat fraction map and histologic examinations of the liver were also performed. In a human study, 14 living liver donors and 11 liver recipients were included and all study subjects underwent CT using dual-energy precontrast imaging, chemical shift MRI for the fat fraction map, and surgery. The CT attenuation values and fat fractions of the DECT, MRI, and pathology results were measured. The Pearson's correlations coefficients were calculated, and Bland-Altman analysis was performed among the fat fractions of DECT, MRI, and pathology. Receiver operating characteristic (ROC) curve analysis was performed to detect $\geq$ 5% or $\geq$ 10% hepatic steatosis.

Results: The CT attenuation of precontrast images showed a strongly negative linear correlation with the histologic HFF. In the animal study, the HFFs of DECT with MMD were strongly correlated with those of pathology and MRI, and the mean differences of the Bland-Altman plots comparing the fat fractions of multiphasic DECT with MMD were very close to zero, even in the presence of iodinated contrast media. However, there was poor agreement between the HFF of DECT with MMD and that of pathology. In the human study, the HFF of DECT with MMD showed good agreement with those of MRI and the pathology results, even though there was no significant linear correlation between the HFF of DECT with MMD and that of pathology. The diagnostic performance of DECT with MMD regarding sensitivity and specificity was comparable to that of precontrast CT and MRI (P = 0.17-0.82).

Conclusions: The quantification of HFF using DECT with MMD is well-correlated and shows good agreement with the HFF of pathology and MRI even in the presence of iodinated contrast media, and has comparable sensitivity and specificity to those of precontrast CT and MRI.

Keywords: dual-energy CT; multi-material decomposition; quantification of hepatic fat fraction; rabbit fatty liver

Student number: 2012-21725

CONTENTS

LIST OF TABLES

LIST OF FIGURES

LIST OF ABBREVIATIONS

DECT = dual-energy CT

SECT = single-energy CT

MMD = multi-material decomposition

MD = two-material decomposition

HFHC = high-fat, high-cholesterol

AP = arterial phase

PVP = portal venous phase

EP = equilibrium phase

HFF = hepatic fat fraction

LFQ = liver-fat quantification

VUE = virtual unenhancement

IOP = in-phase and opposed-phase

IDEAL IQ = iterative decomposition of water and fat using echo-asymmetry and the least-squares estimation quantitative sequence

HU = Hounsfield unit

SI = signal intensity

H&E = Hematoxylin and Eosin

ROC = receiver operating characteristic

AUROC = area under the ROC curve

INTRODUCTION

Hepatic steatosis or fatty liver disease is recognized as the most prevalent liver disease worldwide. The prevalence of this disease is rapidly rising along with the increasing prevalence of obesity and it is being more frequently detected with the increased use of ultrasonography and computed tomography (CT). It is known that this condition increases not only the risk of the development of liver cirrhosis and hepatocellular carcinoma (1-3), but also the risk of mortality after liver resection (4-6). Because the condition can be improved with effective treatment and diet, it is very important to know the extent of the hepatic steatosis, i.e. the content of fat in liver tissue, so that an effective treatment plan can be devised and the treatment results can be evaluated. Hepatic steatosis also influences the outcome of liver transplantation for both the recipient and the living liver donor during the postoperative period (7-9). Severe macrovesicular steatosis (>60%) in donor liver has been associated with a greater than 60% risk of primary non-function after transplantation, and a moderate degree of macrovesicular steatosis (30-60%) in donor livers may also result in decreased hepatocyte regeneration and higher rates of graft dysfunction, non-function, and ischemic injury (10). Therefore, accurate quantification of hepatic steatosis is also critical for the selection of living liver donors.

Histologic examination of hepatocellular fat vacuoles remains the reference standard for the detection and quantification of hepatic steatosis, although liver biopsy is invasive and time-consuming and sampling errors can occur

(11). In addition, routine histologic examination is semiquantitative, observer-dependent, and graded with broad severity brackets (12). Moreover, liver biopsy cannot be repeated often enough in order to monitor the treatment response due to the procedure-related complications and potential morbidity (13). Therefore, an alternative, noninvasive means of diagnosing hepatic steatosis would be beneficial. Noninvasive imaging modalities for diagnosing fatty liver include ultrasonography, magnetic resonance imaging (MRI), and CT. Among these modalities, ultrasonography is the easiest and most widely accepted first imaging technique with the additional benefit of its lack of a radiation hazard, although it is a subjective method and highly operator- and equipment-dependent, so that only a qualitative assessment of the fatty liver is possible (14-19). CT depicts focal fatty infiltration of the liver and the diffuse fatty liver, as showing low attenuation and the degree of decrease in CT attenuation has been shown to be related to the degree of fatty infiltration of the liver (20-25). Although CT is useful for the detection of fatty liver, it has low sensitivity for detecting mild to moderate hepatic steatosis (26, 27) and hemosiderin deposition can preclude an accurate assessment of hepatic steatosis based on CT attenuation (28). MR spectroscopy is able to measure fat and water proton signals and is probably the best method for detecting a small amount of fatty infiltration. As confirmed by biochemical assay of tissue specimens, the fat fraction (FF) calculated from proton densities determined on spectroscopy is equivalent to the tissue triglyceride concentration (12, 29). Recent studies have also demonstrated that low-flip-angle, multiecho, gradient recalled-echo MR imaging with relaxation and interference correction (30) or

T1 independent, T2* corrected chemical shift based fat-water separation with multi-peak fat spectral modeling (31) is a rapid, safe, and highly accurate diagnostic and fat-grading modality for fatty liver disease. However, MR imaging is relatively expensive and limited in its accessibility.

Meanwhile, recent studies also demonstrated that dual-energy CT which involves scanning with two, different tube potentials (typically, 140 and 80kVp), may be used to evaluate hepatic steatosis by measuring the change in hepatic attenuation between images acquired at the lower and higher energy levels (25, 32-34). In the situation of hepatic steatosis without iron overload or iodinated contrast media, two-material decomposition (MD) with basic materials of fat and liver will be able to similarly quantify the degree of hepatic steatosis. As multi-material decomposition (MMD) with three basic materials of fat, liver, and other, such as iron or iodinated contrast media, considers the amount of other material in the liver, it is, therefore, expected that MMD will show better performance in quantifying the degree of hepatic steatosis in the iron overloaded situation or on post-contrast images than MD. MMD is based on the additional assumption of volume conservation (35), however, when grinding and mixing of liver tissue, fat, and iron or other material, the final volume of the mixed material will change and become different with the in-vivo situation. Because the change of total volume of mixed materials is thought to affect the amount of calculated fractions of decomposed materials, an animal or human study using live tissue is needed to evaluate the performance of MMD. If accurate quantification of HFF in postcontrast CT imaging is possible, the precontrast scan could be skipped in

some patients and the exposed radiation dose from CT scanning could be decreased.

Therefore, the purpose of this study is to evaluate the feasibility and accuracy of dual-energy CT (DECT) using multi-material decomposition (MMD) for quantification of the hepatic fat fraction (HFF) and to evaluate the diagnostic performance compared with the precontrast CT number, using the histologic examination as the reference standard and MR fat quantification as the technical standard. Quantification of HFF using CT, which is an objective imaging modality and is widely used with easy accessibility, would be helpful for evaluation of the treatment effect of hepatic steatosis and for preoperative evaluation of living liver donor candidates.

1. ANIMAL STUDY

MATERIALS AND METHODS

Animal model

This study was approved by the Institutional Animal Care and Use Committee of our medical institution (IACUC No. 12-0068 and 13-0021). Sixteen, male, New Zealand White rabbits were randomly divided into four groups. As shown in Figure 1, four rabbits (group 1) were fed a standard diet for six weeks and were used as the control group. Twelve rabbits (groups 2, 3, and 4) were fed a high-fat, high-cholesterol (HFHC) diet (Standard diet + 10% lard + 2% cholesterol + 2% maltose dextrin; Dyets, Bethlehem, PA, USA: product No. 621079) (36). To reach different stages of fatty liver, four rabbits (group 2) were fed a standard diet for four weeks followed by a HFHC diet for two weeks, four rabbits (group 3) were fed a standard diet for two weeks followed by a HFHC diet for four weeks, and four rabbits (group 4) were fed a HFHC diet for six weeks.

Two animals, one from group 3 and the other from group 4, had suffered from anorexia and general weakness, so they did not enough HFHC diet to produce hepatic steatosis. Furthermore, the animal in group 4 of the two animals died during MRI scanning and, therefore, this case was exempted from the fat fraction analysis due to the improper pathologic specimen. All animals in group 1, the control group, showed normal liver histology with the histologic fat fractions being up to 7%. The animals in group 2 (2 weeks of a HFHC diet) had mild to moderate hepatic steatosis, ranging from 20% to 35%

Figure 1. Diet schedule to produce different stages of hepatic steatosis in rabbits of the present study. Group 1 were fed a standard diet for six weeks and were used as the control group. Group 4 were fed a high-fat, high-cholesterol (HFHC) diet (Standard diet + 10% lard + 2% cholesterol + 2% maltose dextrin) for six weeks.

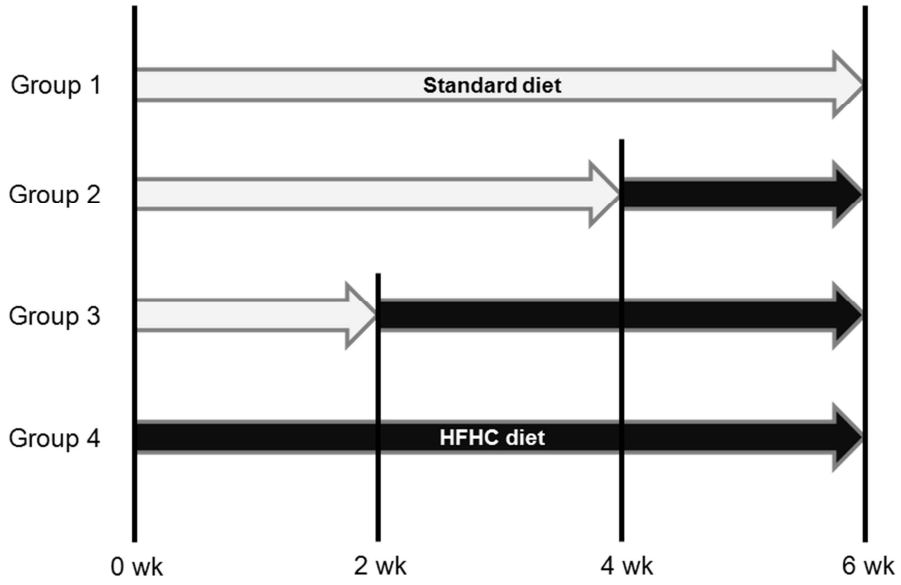

(grade 1-2), according to the histologic exam. Groups 3 and 4 (four and six weeks of a HFHC diet, respectively) showed histologically moderate to severe fatty liver except for the two anorexia cases, and thus ranging from 60% to 87.5% (grade 2-3).

CT acquisition

After the six-week feeding period, single- and dual-energy CT imaging examinations were performed using a single-source, 64-slice MDCT scanner with fast kVp switching technology (Discovery CT750 HD; GE Healthcare). The animals were sedated with an intramuscular injection of 5 mg/kg of a 1:1 combination of tiletamine hydrochloride and zolazepam (Zoletil; Virbac, Carros, France) and xylazine hydrochloride (Rompun 2%; Bayer Korea, Seoul, Korea). Axial images were obtained with the animals in the supine position, and covering the entire liver. The single-energy CT was performed at 120kVp and 400mA and the dual-energy CT was performed at two energy levels of 140kVp, 550 mA and 80kVp, 550 mA. The CT parameters were as follows: collimated slice thickness, 5 mm; pitch, 1; and gantry rotation time of 0.5 seconds. Automatic tube current modulation was not used.

The multiphasic CT protocol consisted of the precontrast, arterial phase, portal-venous phase, and equilibrium phase. The precontrast images were obtained using both single- and dual-energy scans. After the precontrast CT scans of single- and dual-energy were performed and iodinated contrast medium in the amount of 370 mgI/mL (iopromide, Ultravist 370; Bayer Schering, Berlin, Germany) at a dose of 1.5 mL/kg was injected into the ear

vein at a rate of 1.2 ml/s for five seconds using a power injector (Stellant Dual; Medrad, Indianola, PA, USA). Equilibrium-phase images were obtained with single-tube energy of 120kVp, whereas arterial and portal venous phase images were obtained with dual-energy scans. The arterial, portal-venous, and equilibrium-phase scans were obtained 10 seconds, 20 seconds, and 60 seconds, respectively, after the start of contrast-medium administration.

Postprocessing of DECT

After CT data acquisition, the DECT data were used for MD and MMD fat fraction map reconstruction, and material specific images were obtained on a separate workstation (GSI Viewer; GE Healthcare). MD was performed using projection-based methods (37) with fat and soft tissue in the material basis. The MD output consisted of a basic pair of fat and soft-tissue density images. The MMD algorithm used in this study was a liver-fat quantification (LFQ) algorithm using commercially unavailable postprocessing software (Liver Fat Quantification; GE Healthcare). An LFQ algorithm was recently developed using the MMD-based algorithm for direct and accurate liver fat quantification using DECT, with fat, liver tissue, and blood in the material basis (37). For three-material decomposition using only two, different spectral data, one additional condition must be provided to solve for three unknowns. It is an ideal solution assumption that the sum of the volume of the three, constituent materials equals the volume of the mixture (35, 38, 39). In the case of contrast-enhanced DECT data, a virtual unenhancement (VUE) image in which the enhancing effect of the iodine contrast agent has been removed and

replaced by the same volume of blood, was first applied before running the LFQ algorithm. The final output of the LFQ algorithm was the fat-fraction map.

MR acquisition

After the CT scan, MR imaging examinations were performed on a 3T MR imaging system (Magnetom Trio, Siemens Medical Solutions, Erlangen, Germany) using a human knee coil and a 1.5T MR imaging system (SignaHDxt, GE Medical Systems, Milwaukee, WI, USA) using a human cardiac coil on the same day as the CT scan. A bandage for pressing on the abdomen of the animals was used in order to reduce respiratory motion artifacts. A T1-weighted, in-phase and opposed-phase (IOP), spoiled gradient recalled echo sequence was performed on a 3T MR system in the axial plane using the following imaging parameters: repetition time (TR) 6.5 msec; echo times (TE) opposed-phase 2.4 msec; TE in-phase 4.0 msec; echo-train length (ETL) 1; flip angle (FA) 9°; number of excitations (NEX) 10; slice thickness 3.2 mm; matrix 320 x 288; and field of view (FOV) 140 mm. In addition, the iterative decomposition of water and fat using echo-asymmetry and the least-squares estimation quantitative sequence (IDEAL IQ, GE Healthcare) were obtained to estimate the HFF on a 1.5T MR system in the axial plane using the following imaging parameters: TR 16.2 msec; first TE 1.8 msec; echo spacing 2.1 msec; ETL 6; FA 8°; NEX 2; slice thickness 2 mm; matrix 256 x 160; and FOV 230 mm. IDEAL IQ produced T2*-corrected water, T2*-corrected fat, R2* maps, and fat-fraction maps.

Image analysis of CT and MR Imaging

CT imaging – To measure the Hounsfield units (HU) of the CT image series, three circular regions of interests (ROI), 30-40 mm2 in size, were placed on the liver parenchyma of the 70keV DECT portal venous phase image by one blinded radiologist (B.Y.H), taking care to avoid large hepatic vessels and artifacts, i.e. one in the right lobe, one in the left medial lobe, and one in the left lateral lobe, using the gallbladder and left hepatic vein as anatomical landmarks. The ROIs were then copied from the 70keV DECT portal venous phase image and pasted onto the other CT image series, i.e. the precontrast and equilibrium phase with single-energy and the precontrast, arterial phase, and equilibrium phase with dual-energy. The mean HU of the CT image series was recorded. To estimate the HFF from MD, 3D ROI measurement was performed on the MD fat maps (soft tissue) and the MD soft- tissue maps (fat). 2D ROIs were manually drawn on all slices containing the liver using ITK-SNAP version 2.2.0 (40). The voxels corresponding to these ROIs were combined to form a 3D ROI, and the mean was calculated from these voxels. Fat fractions of MD were calculated using the following formula: (value of fat density image) / (value of fat density image + value of soft tissue density image) (37). HFF of MMD was also measured by 3D ROI measurement method, as described above.

MR Imaging – On MR images, ROIs were defined on the in-phase image series in the manner used in measuring the HU of CT images, and was then copied from the in-phase images and pasted onto the opposed-phase images

and the IDEAL T2*-corrected fat-fraction images. Signal intensity (SI) decrease on opposed-phase images compared with in-phase images was calculated using the following formula: SIin−SIout/2⊥|SIin (19), and ROI measurements of the HFF on the IDEAL fat-fraction images were recorded. The average of the three ROI measurements for each series of MR imaging was used as a representative value.

Histologic analysis

After the MRI exam, all animals were sacrificed by intravenous injection of 3 mL of KCl under deep anesthesia. The liver tissue specimens were obtained from four parts of the liver, i.e. right posterior, right anterior, left medial, and left lateral segments. All tissue specimens were fixed in 10% formalin for 48 hours, embedded in paraffin, cut into 5-um thick slices, and stained with Hematoxylin and Eosin (H&E). The degree of fat accumulation was reviewed in H&E-stained preparations by one blinded pathologist (K.B.L, 11 years of clinical experience conducting hepatic pathologic examinations). As fat accumulation was observed as vacuoles in hepatocytes in these preparations, the degree of fat accumulation was quantitatively assessed by the degree of vacuolation using the percentage of volume of fat vacuoles over the total volume of hepatocytes. The degree of fat accumulation was also classified into four, semi-quantitative groups: normal being less than 5%; mild between 5% and 33%; moderate between 33% and 66%; and severe with more than 66% of fat vacuoles within the cytoplasm of the hepatocytes, according to the steatosis score of the NAFLD activity score (NAS) system (41).

Statistical analysis

The one-way analysis of variance (ANOVA) test was used for the intergroup comparison of the CT Hounsfield unit data and the HFF analysis among the four animal groups. When statistically significant differences occurred, single post-test comparisons were performed using the Tukey post-hoc comparison tests with Bonferroni correction for multiple comparisons. The Pearson correlation coefficient and the paired t test were used for statistical analysis to determine the correlation between the HFFs of multiphasic DECT data, MRI with IDEAL IQ and IOP, and pathologic steatosis. Bland–Altman analysis was also used to determine the agreement among the HFFs of DECT, MRI IDEAL IQ, and the pathology results. In addition, receiver operating characteristic (ROC) curve analysis was performed to evaluate the diagnostic performance and to determine the optimal cutoff values of the CT attenuation value of precontrast SECT, HFFs of DECT with MMD, and MRI IDEAL IQ, for identifying the presence of hepatic steatosis or substantial steatosis. Substantial steatosis was defined as >10% steatosis as this criterion was considered as requiring further evaluation or dietary intervention before liver donation. The optimal cutoff value was defined as the value at which the sum of the sensitivity and specificity was maximized. All statistical analyses were performed using commercially available software (SPSS, version 21.0; SPSS, Chicago, IL, USA). A P value less than 0.05 was considered to indicate statistical significance.

1. ANIMAL STUDY

RESULTS

CT attenuation coefficients

As expected, there were significant differences regarding the CT attenuation values of the precontrast images among the four groups (P = <0.001 for SECT; P = 0.002 for DECT), while there was no significant difference among the four groups in terms of the CT attenuation values of all of the post-contrast image sets (P = 0.231-0.997). When comparing the CT values of the precontrast image sets, i.e. 120kVp image of SECT and 70keV image of DECT, there was no significant difference (P = 0.163).

The CT attenuation values of the precontrast images showed a strongly negative linear correlation with the histologic HFF (r = -0.868 and P < 0.001 for SECT; r = -0.889 and P < 0.001 for DECT). On the other hand, there was no significant correlation between the CT value of the post-contrast image sets and the histologic HFF (P = 0.234-0.365).

Correlation of measured HFFs of DECT and MRI with pathology

Table 1 shows the measured HFF values of pathology, multiphasic DECT, and MRI for each animal. The HFF results using MD of post-contrast DECT data were negative values which could not have actually occurred. Therefore, we did not consider the MD results of post-contrast DECT in Table 1 and the following correlation analysis.

Table 1. Hepatic fat fraction values of pathology, DECT using MMD or MD, and MRI of each animal

Animal ID	HFHC diet (weeks)	Pathology (%)	MMD, pre (%)	MMD, AP (%)	MMD, PVP (%)	MMD, EP (%)	MD, pre (%)	MRI, IDEAL (%)	MRI, IOP (%)
101	0	<5	1.0	0.7	1.1	0.7	13.2	3	6.7
102	0	<5	1.5	1.6	1.7	2	14.6	3	3.8
103	0	6.0	2.2	2.7	1.9	2	16.1	3	5.6
104	0	7.0	0.5	0.6	0.2	0.5	17.3	2	3.4
201	2	25.0	6.7	6.5	6.2	6.6	21.3	9	9.5
202	2	32.5	6.7	7.0	4.7	6.4	22.9	8	8.2
203	2	35.0	6.4	5.4	4.0	6.1	23.0	8	11.8
204	2	20.0	8.6	7.2	6.4	6.3	21.3	9	6.8
301	4	68.3	15.6	15.3	14.2	14.7	32.2	15	16.5
302	4	60.0	20.9	20.4	18.4	19.4	23.1	8	8.85
303	4	5.0	12.6	11.3	13.8	14.6	15.4	5	3.2
304	4	77.5	22.0	19.6	19.2	19.3	32.4	11	12.2

401	6	72.5	12.4	13.1	10.4	11.8	30.1	9	10.3
402	6	87.5	20.6	19.4	15.9	17.3	32.2	11	8.4
403	6	67.5	19.5	17.8	16.3	16.4	21.1	7	61.
404	6	-	17.1	16.7	15.2	15.4	19.5	5	3.1

Note.— MMD = multi-material decomposition, MD = material decomposition, DECT = dual-energy CT, AP = arterial phase, PVP = portal venous phase, EP = equilibrium phase, IDEAL = iterative decomposition of water and fat using echo-asymmetry and the least-squares estimation quantitative sequence, IOP = in-phase and opposed-phase

The HFF using MMD of precontrast DECT was significantly higher than that of the post-contrast DECT image sets which were obtained in the arterial, portal venous, and equilibrium phases ($P < 0.05$). However, the mean differences of the Bland-Altman plots comparing the MMD fat fractions of precontrast and post-contrast DECT data were -0.6% in the arterial phase, -1.5% in the portal venous phase, and -0.9% in the equilibrium phase, and which were close to zero, as shown in Figure 2.

The HFFs measured by multiphasic DECT using either MMD or MD, were strongly correlated with the histologic HFF ($P <0.001$). The correlation coefficients of the MMD fat fraction results of the four phases were similar to each other ($r = 0.854$ of precontrast, $r = 0.874$ of the arterial phase, $r = 0.794$ of the portal-venous phase, and $r = 0.813$ of the equilibrium phase; $P < 0.001$ of all phases), and the correlation coefficient of the MD fat fraction of precontrast DECT showed the highest value ($r = 0.929$, $P < 0.001$). The measured HFFs of multiphasic DECT with MMD were also strongly correlated with that of MR IDEAL IQ ($r = 0.652$ - 0.896, $P < 0.01$), whereas there was no significant correlation between the HFFs of multiphasic DECT and MR IOP ($P = 0.082$-0.132). The HFFs measured by IDEAL IQ and IOP were strongly correlated with that of pathology ($r = 0.834$ of IDEAL IQ, $r = 0.716$ of IOP; $P < 0.001$). Figure 3 shows the scatter charts of HFFs of precontrast DECT with MMD, MR IDEAL IQ, and pathology. The linear regression equations were obtained of these measured HFFs. The equation of the HFFs of precontrast DECT with MMD (X) and HFFs of pathology (Y) was: $Y = 3.62X + 1$.

Figure 2. Bland-Altman plots of the fat fractions (%) of DECT with MMD of pre- and AP (a), pre- and PVP (b), and pre- and EP (c). pre = precontrast, AP = arterial phase, PVP = portal venous phase, EP = equilibrium phase. These results indicate good agreement among the MMD fat fractions of multiphasic DECT, even in the presence of iodinated contrast media.

(a)

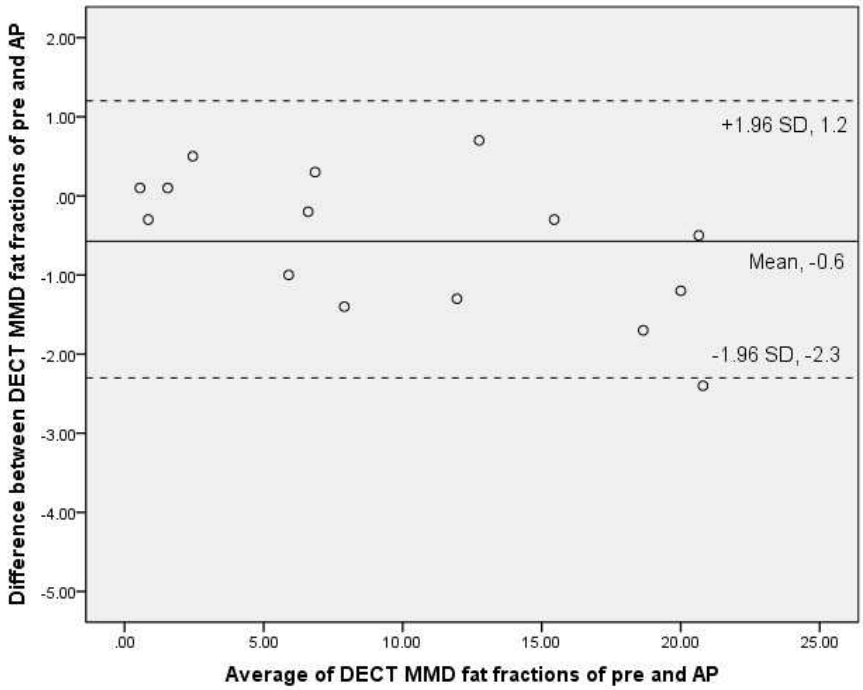

(b)

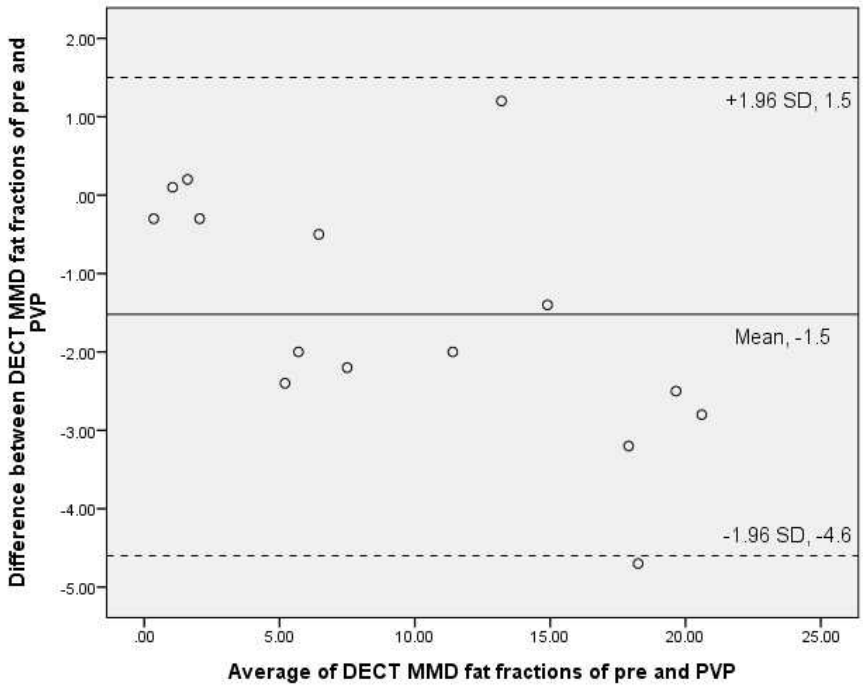
Difference between DECT MMD fat fractions of pre and PVP
2.00
1.00
.00
-1.00
-2.00
-3.00
-4.00
-5.00
+1.96 SD, 1.5
Mean, -1.5
-1.96 SD, -4.6
.00
5.00
10.00
15.00
20.00
25.00
Average of DECT MMD fat fractions of pre and PVP

(c)

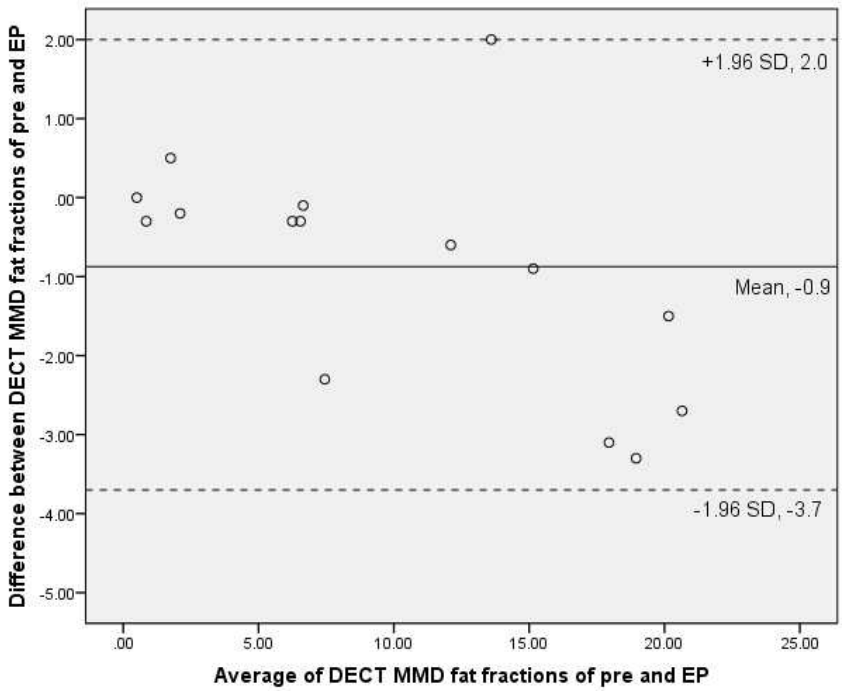
Difference between DECT MMD fat fractions of pre and EP
2.00
1.00
.00
-1.00
-2.00
-3.00
-4.00
-5.00
+1.96 SD, 2.0
Mean, -0.9
-1.96 SD, -3.7
.00
5.00
10.00
15.00
20.00
25.00
Average of DECT MMD fat fractions of pre and EP

Figure 3. Correlation of the hepatic fat fraction values between (a) precontrast DECT with MMD and MR IDEAL IQ, (b) precontrast DECT with MMD and pathology, and (c) MR IDEAL IQ and pathology. There are strong correlations between the hepatic fat fractions of DECT, MRI, and pathology.

(a)

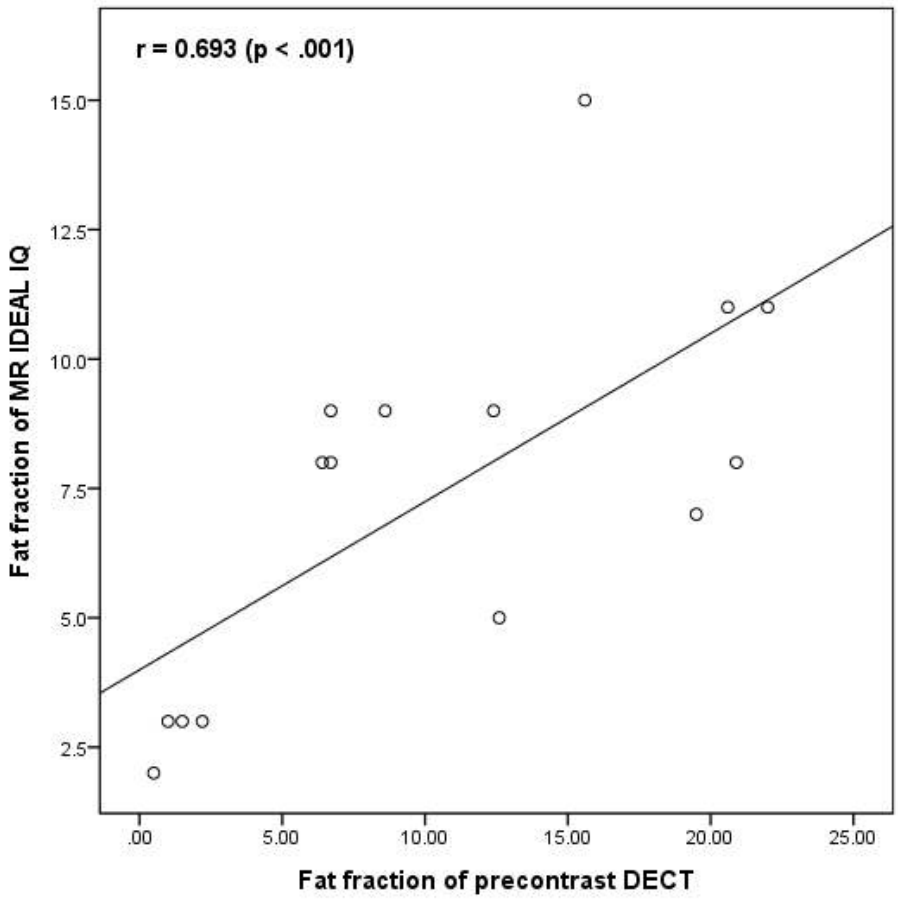

(b)

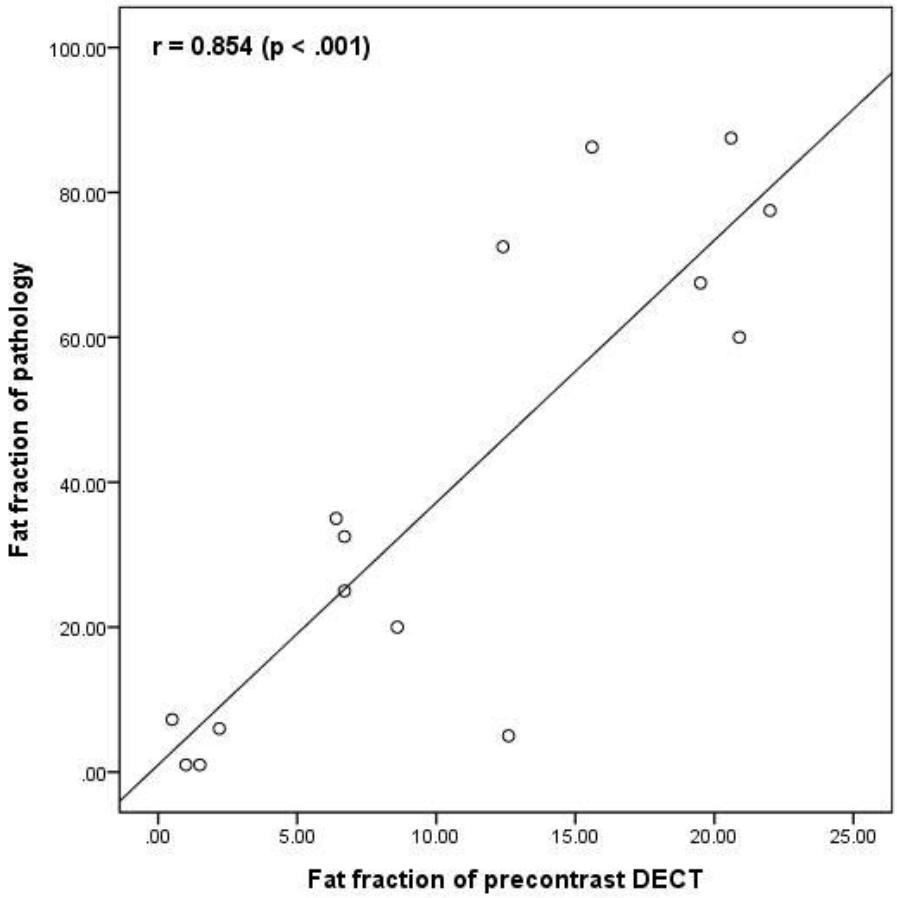
r = 0.854 (p < .001)
100.00
80.00
60.00
40.00
20.00
.00
Fat fraction of pathology
.00
5.00
10.00
15.00
20.00
25.00
Fat fraction of precontrast DECT

(c)

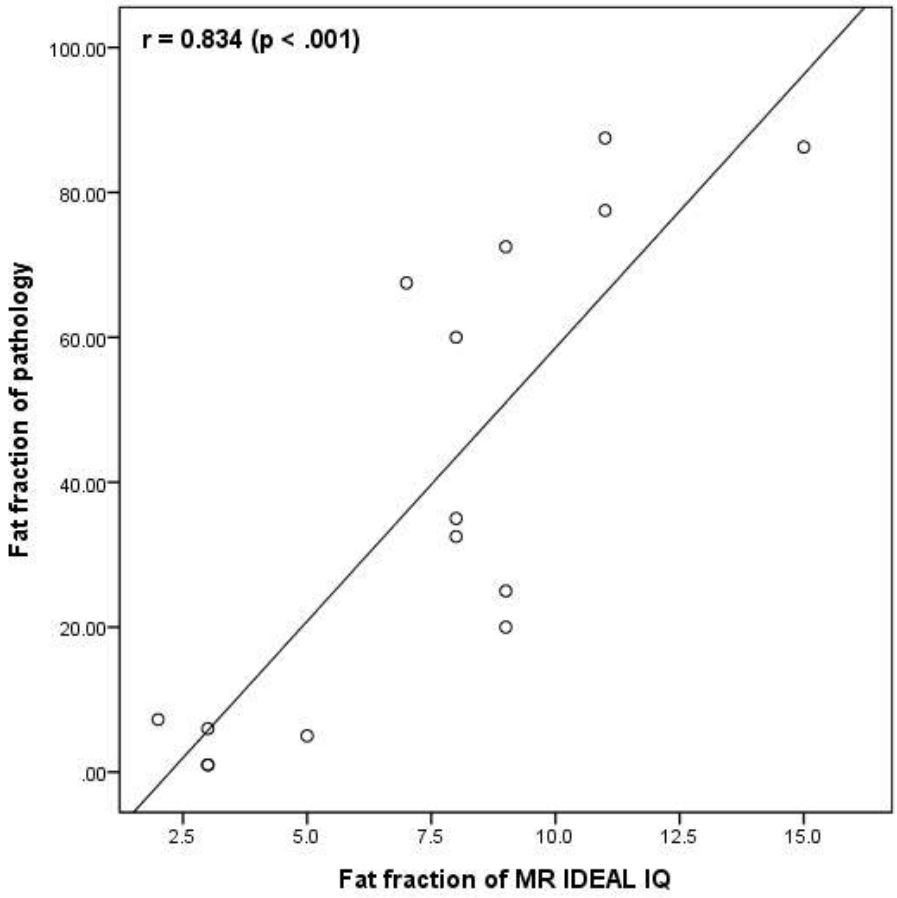
r = 0.834 (p < .001)
100.00
80.00
60.00
40.00
20.00
.00
Fat fraction of pathology
2.5
5.0
7.5
10.0
12.5
15.0
Fat fraction of MR IDEAL IQ

The Bland-Altman plots comparing the HFFs of MMD of precontrast DECT and MR IDEAL IQ showed a mean difference of 3.1%, which did not differ significantly from zero, while comparison of the fat fractions of MMD of precontrast DECT and pathology was -28.4%, thus indicating poor agreement between the two measurements. The Bland-Altman plot comparing HFFs of MR IDEAL IQ and pathology also showed a mean difference of -31.5%, similar to the mean difference of the Bland-Altman plot comparing the HFFs of DECT with MMD and pathology (Figure 4).

The CT and MRI of representative subjects in groups 1 and 4 are shown in Figures 5 and 6, respectively.

Figure 4. In the animal study, Bland-Altman plots of the fat fractions (%) of DECT with MMD and MR IDEAL (a), the fat fractions of DECT with MMD and the pathology results, and the fat fractions of MR IDEAL and pathology results (c). These results indicate that the fat fraction of DECT MMD is comparable with that of MR IDEAL for the quantitative estimation of hepatic steatosis, however, the fat fraction of DECT MMD and MR IDEAL differ from that of the pathology results.

(a)

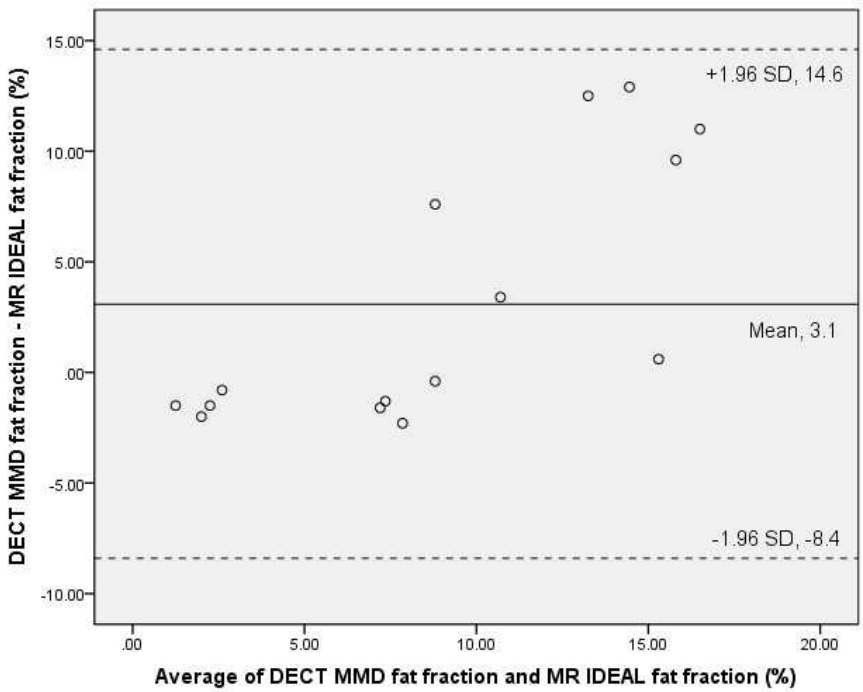

(b)

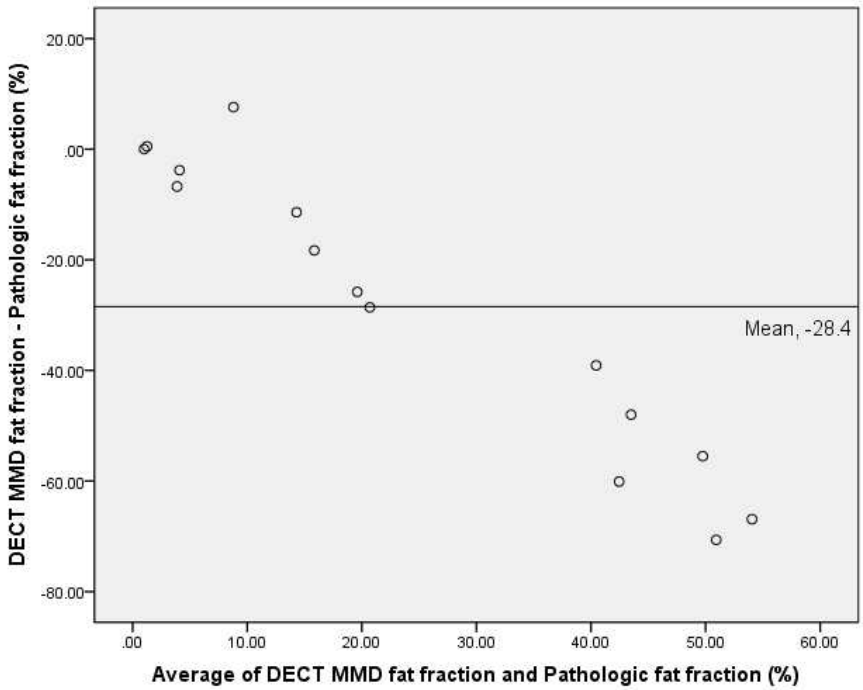
20.00
.00
-20.00
-40.00
-60.00
-80.00
DECT MMD fat fraction - Pathologic fat fraction (%)
Mean, -28.4
.00
10.00
20.00
30.00
40.00
50.00
60.00
Average of DECT MMD fat fraction and Pathologic fat fraction (%)

(c)

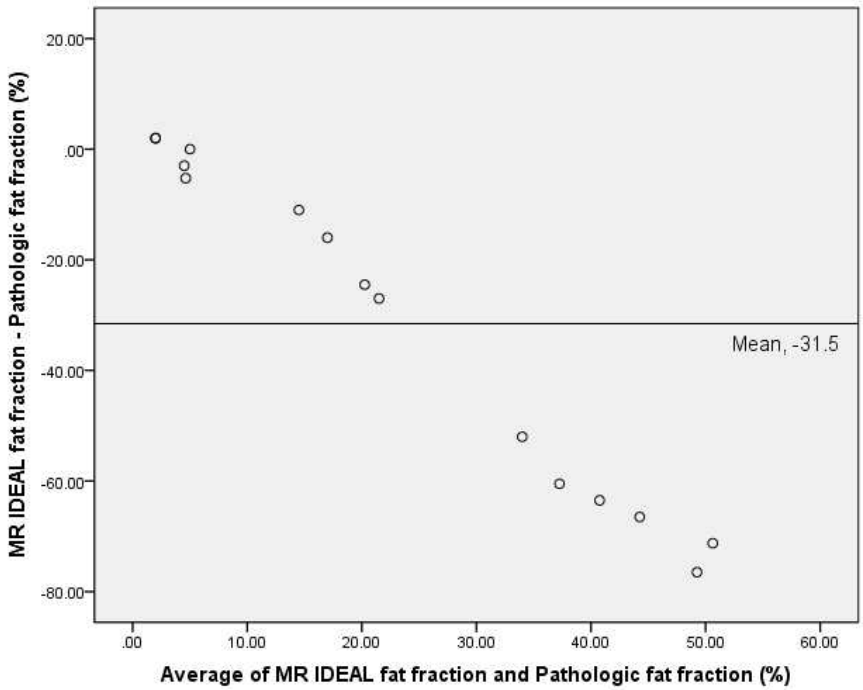
20.00
.00
-20.00
-40.00
-60.00
-80.00
MR IDEAL fat fraction - Pathologic fat fraction (%)
Mean, -31.5
.00
10.00
20.00
30.00
40.00
50.00
60.00
Average of MR IDEAL fat fraction and Pathologic fat fraction (%)

Figure 5. Representative case in group 1 of the animal study, in which the animals were fed a standard diet for six weeks as the control group. (a) precontrast, single-energy CT image, (b) fat fraction maps from IDEAL IQ, (c) MMD fat fraction map of precontrast DECT, and (d) MMD fat fraction map of portal phase DECT. The hepatic HU of (a) was 60.0 and the measured fat fractions of (b-d) were 3.0, 2.2, and 1.9 respectively. (e) Gross specimen of the liver and (f) high-power photomicrograph with hematoxylin-eosin stain. Note that there was no fatty infiltration in the liver.

(a)

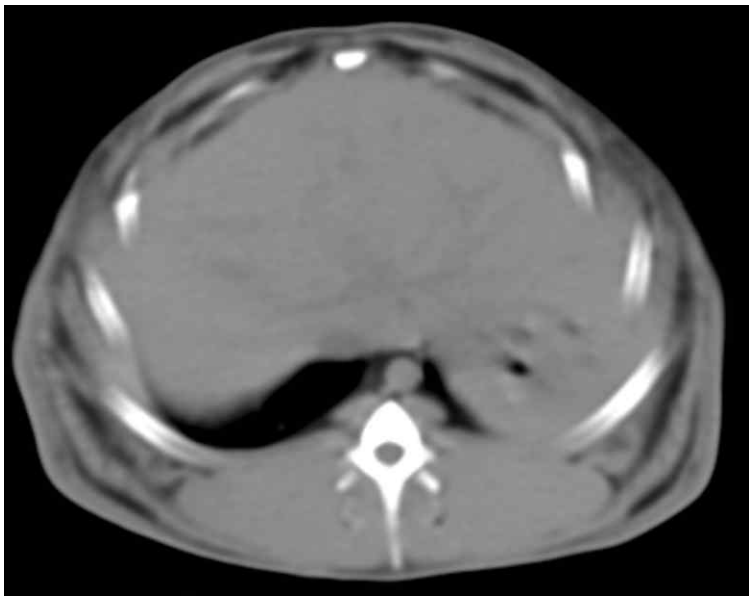

(b)

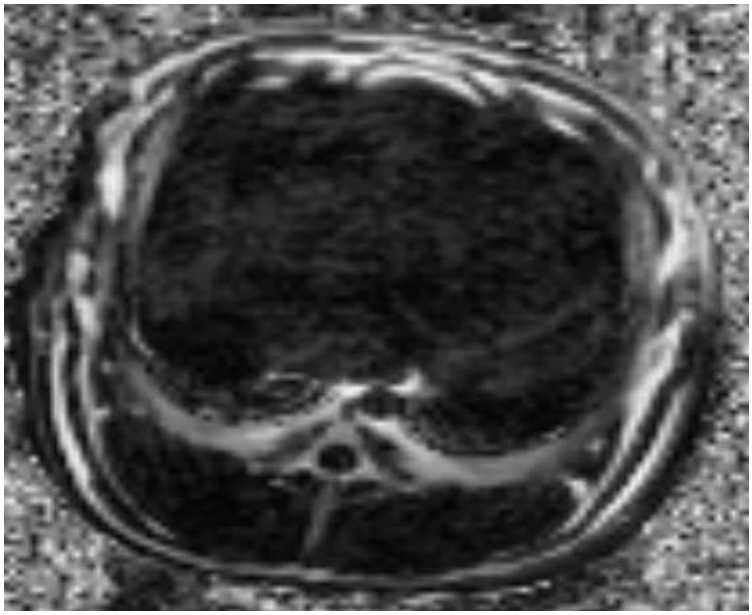

(c)

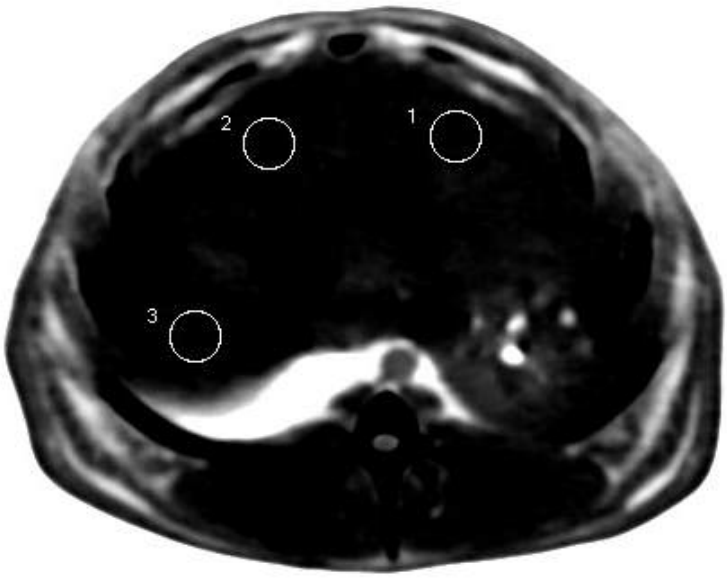

(d)

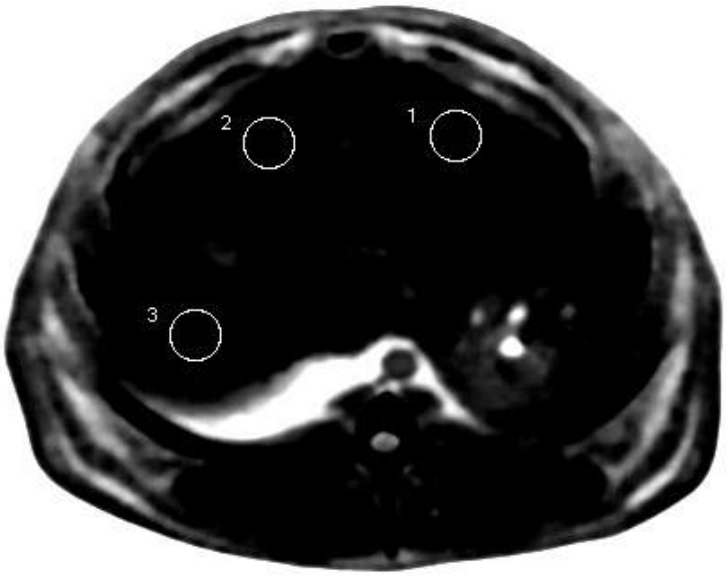

(e)

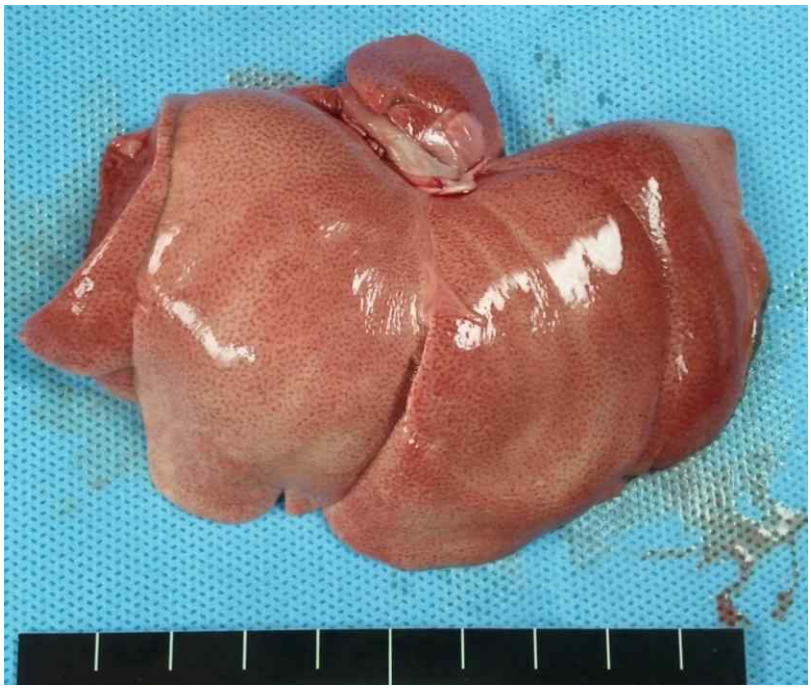

(f)

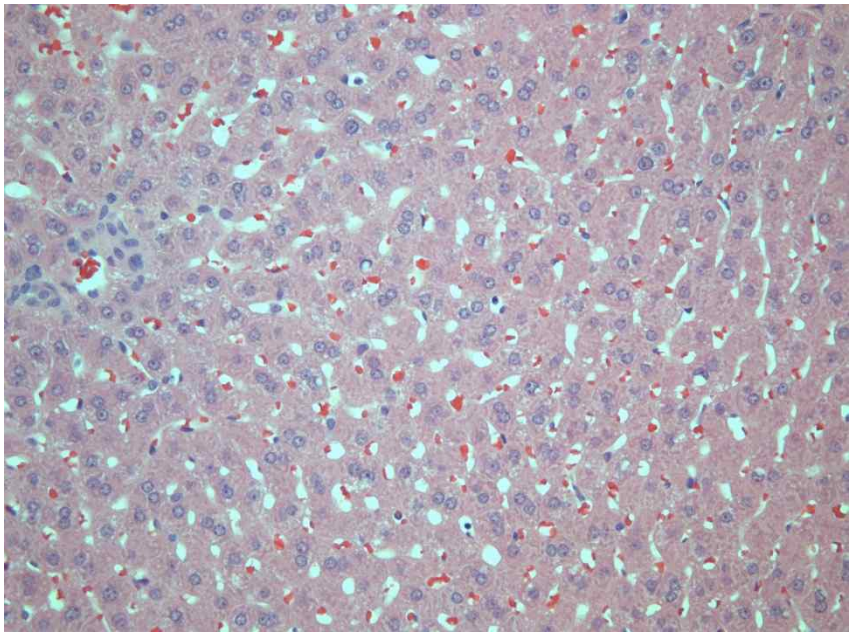

Figure 6. Representative case in group 4 of the animal study, and which was fed a high-fat, high-cholesterol diet for six weeks. (a) precontrast single-energy CT image, (b) fat fraction maps from IDEAL IQ, (c) MMD fat fraction map of precontrast DECT, and (d) MMD fat fraction map of portal phase DECT. The hepatic HU of (a) was 31.5 and the measured fat fractions of (b-d) were 11.0, 20.6, and 15.9 respectively. (e) Gross specimen of the liver and (f) high-power photomicrograph with hematoxylin-eosin stain. Diffuse severe fatty infiltration was noted in the liver.

(a)

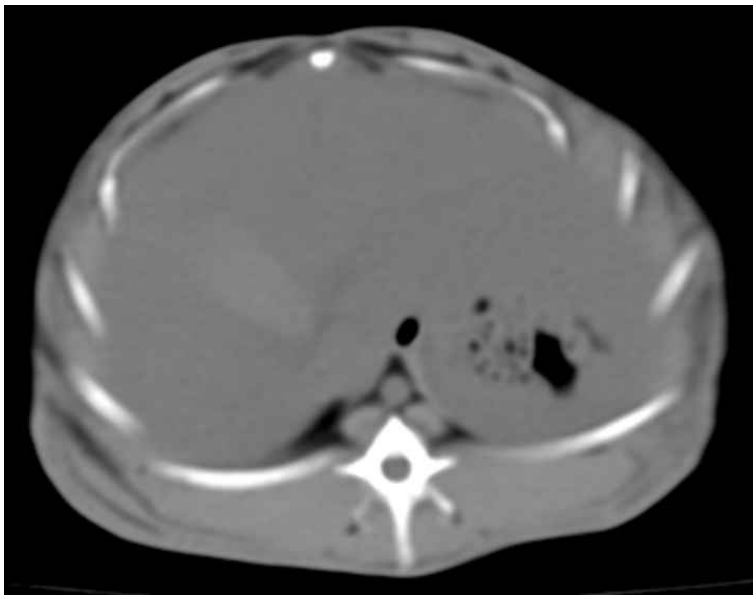

(b)

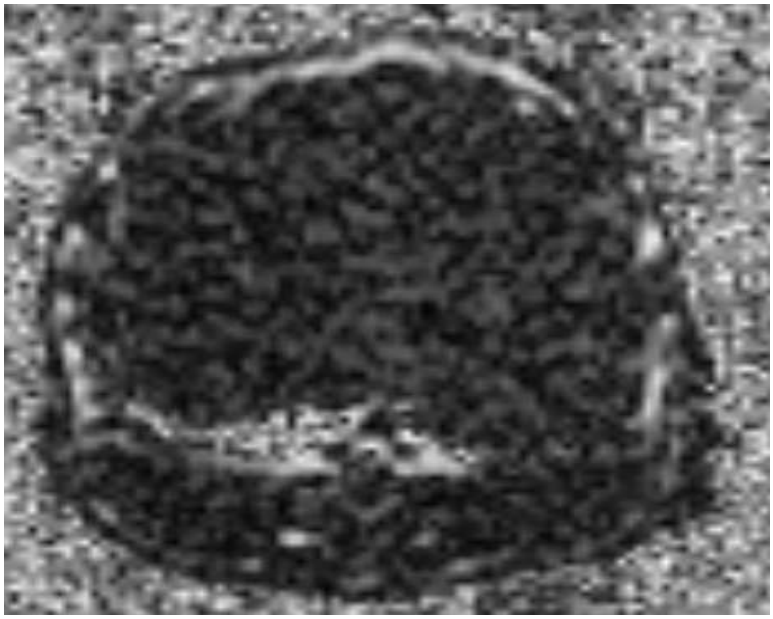

(c)

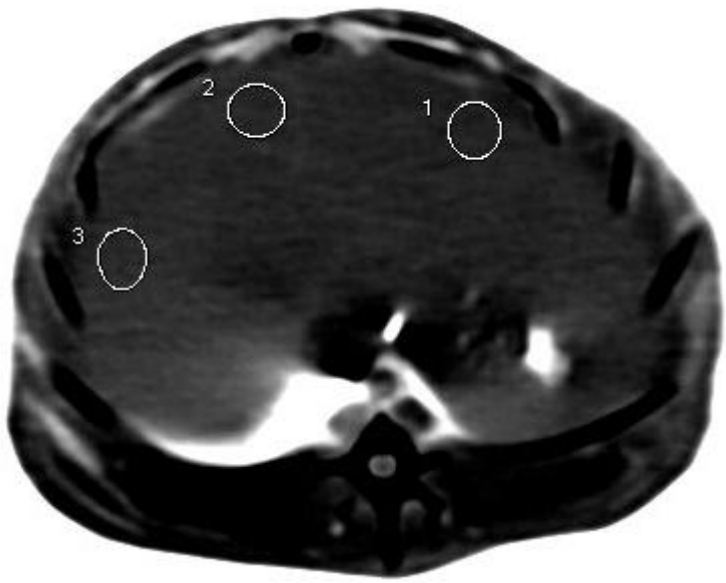

(d)

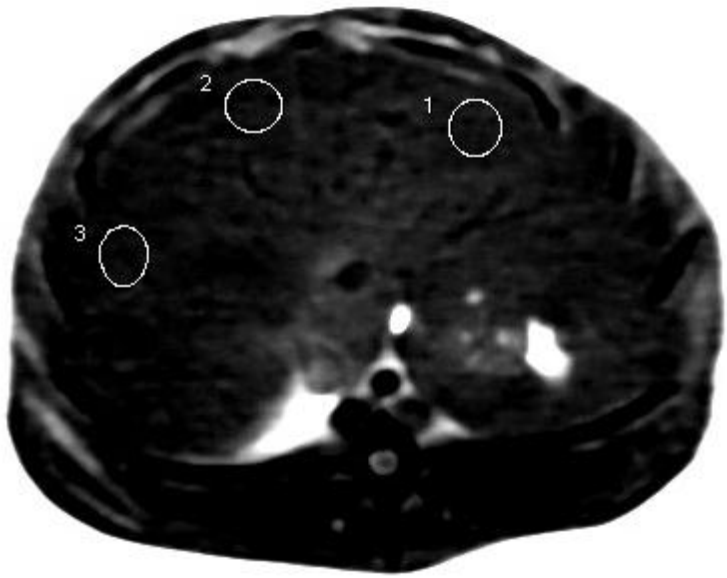

(e)

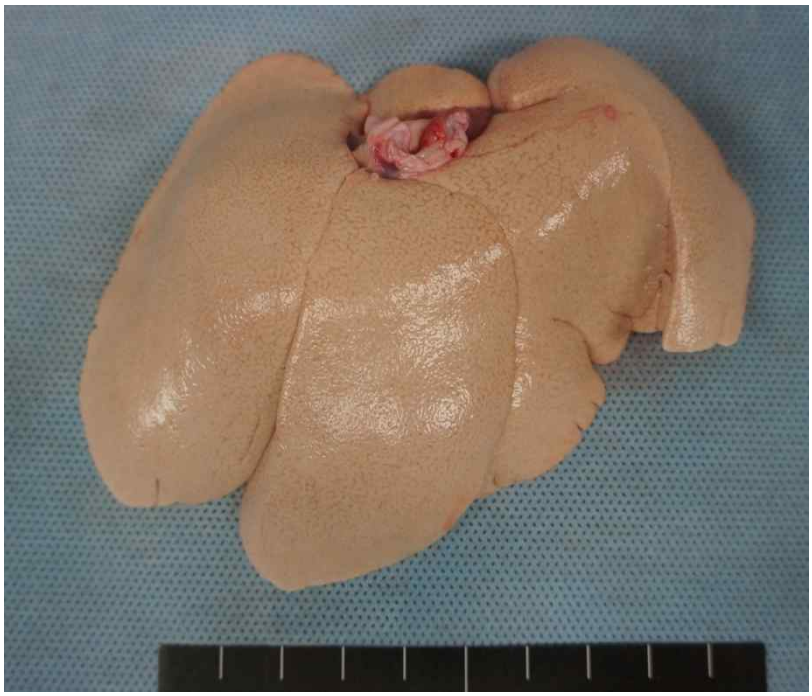

(f)

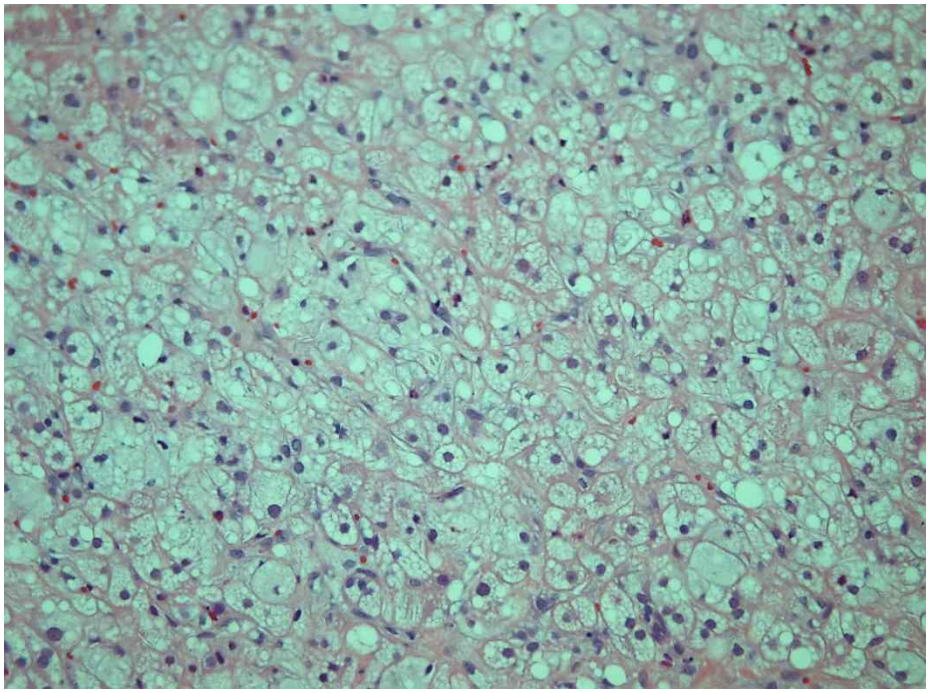

Diagnostic Performance of DECT with MMD for detecting hepatic steatosis

When the cutoff value for the CT number of precontrast SECT was set at 60 HU for the diagnosis of more than 5% hepatic steatosis, the area under the ROC curve was 0.962 (95% CI, 0.721-1.000) with a sensitivity of 92.3% and specificity of 100%. And when the cutoff value of HFF for the diagnosis of more than 5% hepatic steatosis was set at 1.5% for DECT with MMD and at 3% for MR IDEAL IQ, the areas under the ROC curves were 0.923 (95% CI, 0.667-0.997) and 0.885 (95% CI, 0.617-0.989), respectively. The DECT with MMD showed 92.3% sensitivity and 100% specificity, and MR IDEAL IQ showed 84.6% sensitivity and 10% specificity for detecting more than 5% hepatic steatosis. The DECT with MMD showed the same sensitivity as that of the precontrast SECT. Although the DECT with MMD provided higher sensitivity than MR IDEAL IQ for detecting more than 5% hepatic steatosis, there was no statistical difference of the area under the ROC curves between the methods (P = 0.317). For the diagnosis of more than 10% hepatic steatosis, the cutoff values were set at 52.5 HU for precontrast SECT, 2.2% for the fat fraction of DECT with MMD, and 5% for the fat fraction of MR IDEAL IQ. The sensitivities and specificities are 90% and 100% for precontrast SECT and and 100% and 80% for the fat fraction of DECT with MMD and MR IDEAL, respectively. The diagnostic performance of DECT with MMD for more than 10% hepatic steatosis was the same with that of MR IDEAL IQ. Table 2 shows the summary of the diagnostic performance and the cutoff values of the ROC analysis in the animal study.

Table 2. Summary of the diagnostic performance and cutoff values of the CT number of SECT, and the fat fractions of DECT with MMD and MR IDEAL for detecting more than 5% or 10% hepatic steatosis, in the animal study.

	Modality	AUROC	Criterion	Sensitivity	Specificity
≥5% hepatic steatosis	**SECT**	0.962 (0.721 - 1.000)	60	92.3%	100%
	DECT with MMD	0.923 (0.667 - 0.997)	1.5	92.3%	100%
	MR IDEAL	0.885 (0.617 - 0.989)	3	84.6%	100%
≥10% hepatic steatosis	**SECT**	0.980 (0.749 - 1.000)	52.5	90.0%	100%
	DECT with MMD	0.900 (0.637 - 0.993)	2.2	100%	80%
	MR IDEAL	1.000 (0.782 - 1.000)	5	100%	80%

Note – Number in parentheses are the 95% confidence interval values; SECT = single-energy CT, DECT = dual-energy CT, MMD = multi-material decomposition, IDEAL = iterative decomposition of water and fat using echo-asymmetry and the least-squares estimation quantitative sequence, AUROC: area under the ROC curve

2. HUMAN STUDY

MATERIALS AND METHODS

Patients

This study was approved by our Institutional Review Board (IRB No. H-1202-086-398). From November 2012 to July 2013, 27 potential liver donors and 18 potential liver recipients were included in this study and had undergone liver CT according to the liver donor protocol and liver recipient protocol, respectively. Of these 45 patients, 20 were excluded from the study because they did not undergo MR imaging or surgery due to various causes including 1) anatomical variation of the hepatic vessels or bile duct or the presence of another donor with more suitable anatomy (n = 13), 2) dual energy CT data were not available (n = 4) or 3) economic problems (n = 3). Finally, 14 living liver donors (seven males and seven females; mean age, 32.9 years; age range, 20-51 years) and 11 liver recipients (seven males and four females; mean age, 53.7 years; age range, 42-65 years) were included in our study. All subjects underwent CT with dual-energy precontrast imaging, MRI, and hepatectomy surgery for liver recipients and right hemihepatectomy for liver donors.

CT acquisition

All patients underwent multiphasic liver CT using a single-source, 64-slice MDCT scanner with a fast kVp switching technology (Discovery CT750 HD; GE Healthcare). The multiphasic liver CT protocol consisted of precontrast,

early arterial phase, portal venous phase, and equilibrium phases. The precontrast images were obtained using a dual-energy protocol at two energy levels of 140kVp and 80kVp with 375 mA and 5–mm, collimated slice thickness. The arterial, portal-venous, and equilibrium phases were obtained using a single-energy protocol at 120kVp with 350 mA and 1.25-mm collimated slice thickness. The other CT parameters were as follows: pitch, 1; gantry rotation time of 0.5 seconds; and noise index, 15. The automated tube current modulation (ATCM, Auto mA 3D; GE Healthcare) program was used.

After the precontrast CT scanning was performed, iodinated contrast medium in the amount of 370 mgI/mL (iopromide, Ultravist 370; Bayer Schering, Berlin, Germany) at a dose of 1.5 mL/kg (555 mgI/kg) per body weight, was injected for 30 seconds using a power injector (Stellant Dual; Medrad, Indianola, PA, USA) and was followed by an injection of 30-40 mL of normal saline. The timing for the arterial phase scanning was determined using the bolus tracking technique; i.e. arterial-phase scanning was automatically started after five seconds for the donor protocol and after 17 seconds for the recipient protocol after the attenuation coefficient of the abdominal aortic blood reached 100 HU at 120kVp. Portal-venous phase and equilibrium-phase scanning were obtained 45 seconds and 2-3 minutes, respectively, after the start of contrast-medium administration. Arterial, portal, and equilibrium-phase images were part of the CT protocol, although they were not analyzed in this study.

The LFQ algorithm was used to obtain the HFF map from precontrast DECT data, as described above in the animal study.

MR imaging acquisition

MR imaging examinations for 14 living liver donors were performed on a 3T MR imaging system (Magnetom Verio, Siemens Medical Solutions, Erlangen, Germany) using a 32-channel, phase-array torso coil and a 1.5T MR imaging system (SignaHDxt, GE Medical Systems, Milwaukee, WI, USA) using an 8-channel, torso phased-array coil. The IDEAL IQ was obtained for the fat fraction map acquisition on the 1.5T MR system in the axial plane using the following imaging parameters: TR 12.3 msec; first TE 0.9 msec; echo spacing 1.8 msec; ETL 6; FA 7°; NEX 2; slice thickness 6 mm; matrix 256 x 160; and FOV 350 mm. IDEAL IQ produced T2*-corrected water, T2*-corrected fat, R2* maps, and fat-fraction maps. The 11 liver recipients underwent MR imaging on a 1.5T MR imaging system (SignaHDxt, GE Medical Systems, Milwaukee, WI, USA) using an 8-channel, torso phased-array coil. The IDEAL IQ was obtained as described above. The mean time interval between CT imaging and MR imaging was 10 days with a range of 0-50 days.

Image analysis

To estimate the HFF, ROI measurement was performed by one blinded radiologist (B.Y.H). Hepatic ROIs were chosen so as to be approximately 200 mm2 in size and avoiding visible blood vessels, focal hepatic lesions, and artifacts. On each image series, 15 ROI measurements (three ROIs per slice x 5 levels) were selected in the right lobe of the liver. On CT images, ROIs

were placed on the 70keV precontrast image and the ROI positions were kept constant on the MMD fat map of DECT by applying a copy-and-paste function at the workstation. The HUs of the 70keV precontrast image and the ROI values of the fat map were recorded. The estimated histologic fat fraction was also calculated using the equation of the HFFs using the MMD of precontrast DECT (X) and the fat fraction of pathology (Y), which was suggested in the aforementioned animal experiment: $Y = 3.62X + 1$. On MR images, ROIs were defined on the IDEAL T2*-corrected fat-fraction images in the manner used for measuring the HU of CT images, and the ROI values of the fat-fraction map were recorded. The average of the ROI measurements for each series was used as a representative value, and the fat fractions obtained from CT and MR imaging were converted into four, semiquantitative classifications according to the steatosis score of the NAS system.

Histologic analysis

The mean of the time interval between CT imaging and surgery was 28.7 days (range, 1-93 days) and that between MR imaging and surgery was 21.9 days (range, 2-93 days). The surgical hepatic specimens were taken from the right hepatic lobe, and all specimens were stained with H&E. The blinded pathologists reviewed the pathology slides to evaluate the degree of steatosis, and that pathologic report was retrospectively reviewed. The degree of macrovesicular and microvesicular steatosis was subjectively and quantitatively assessed using the percentage of hepatocytes containing intracellular fat, as calculated on H&E staining. The degree of hepatic

steatosis was also classified into four, semi-quantitative groups, with normal being less than 5%, mild between 5% and 33%, moderate between 33% and 66%, and severe with more than 66% of the hepatocytes having fat vacuoles within the cytoplasm, according to the steatosis score of the NAS system.

Statistical analysis

To determine the correlation between the HFFs of DECT, MRI IDEAL, and pathologic steatosis, the Pearson correlation coefficient was used for statistical analysis. The cross-correlation analysis and chi-square test were used for correlation analysis between the hepatic steatosis classifications of DECT, MRI IDEAL, and pathology. Bland–Altman analysis was also used to determine the agreement among the HFFs of DECT, MRI IDEAL, and the pathology results. As in the animal experiment, ROC curve analysis was performed to evaluate the diagnostic performance and to determine the optimal cutoff values of the CT attenuation value of precontrast SECT, HFFs of DECT with MMD, and MRI IDEAL IQ for identifying the presence of hepatic steatosis or substantial ($\geq$ 10%) steatosis. The optimal cutoff value was defined as the value at which the sum of the sensitivity and specificity was maximized. All statistical analyses were performed using commercially available software (SPSS, version 21.0; SPSS, Chicago, IL, USA). A P value less than 0.05 was considered to indicate statistical significance.

2. HUMAN STUDY

RESULTS

Histopathologic results of hepatic steatosis

In the liver donor group, the hepatic steatosis scores of 11 donors were normal and those of the other three donors were of a mild degree. Among the three liver donors with mild hepatic steatosis, one showed 5% HFF in the pathology results and also 5% HFF of MR IDEAL IQ. Another liver donor with mild hepatic steatosis had undergone liver biopsy because 13.7% of HFF was suggested on preoperative MR IDEAL IQ, and 10% of histologic HFF was confirmed by the liver biopsy. This liver donor went on a diet and exercised for about two weeks so that the final pathologic fat fraction of the surgical specimen was less than 5%. The fat fraction of the last remaining liver donor with mild hepatic steatosis was underestimated preoperatively as 4.2%, while the final pathologic fat fraction was 20% (5% macrovesicular fatty change of the total volume of hepatic parenchyme and 15% microvesicular fatty change of the total number of hepatocytes). In the liver recipient group, there were six with no fatty change, three with a mild degree, and two with a moderate degree of hepatic steatosis, while there was no moderate degree of hepatic steatosis in the preoperative imaging study. Overall, according to the pathologic steatosis score, there were 17 with normal liver, six with a mild degree, and two with a moderate degree of hepatic steatosis.

Correlation between HFFs of DECT with MMD and MR with pathology

The CT attenuation value of the 70keV precontrast image of DECT showed a negative linear correlation with the histologic HFF (r = -0.427 and P = 0.033). However, there was no significant linear correlation between the HFF of DECT with MMD and that of histology (P = 0.082), and also between the equation-based estimated HFF of DECT with MMD and the histologic HFF (P = 0.082). The fat fraction of MR IDEAL IQ showed a positive correlation with that of DECT with MMD (r = 0.483 and P = 0.014) and that of histology (r = 0.525 and P = 0.007). In the cross-correlation analysis regarding the steatosis score of the NAS system, DECT with MMD showed no significant correlation with the histologic result (P = 0.206) and MR IDEAL IQ (P = 0.070), although there was a significant correlation between the equation-based estimated fat fraction of DECT with MMD and the fat fraction of histology (P = 0.014) and MR IDEAL IQ (P = 0.027).

Figure 7 shows the Bland-Altman plots between the HFFs of DECT, MRI, and pathology. The Bland-Altman plot comparing the fat fraction of DECT with MMD and that of MR IDEAL IQ showed a mean difference of 0.7%, and comparison of the fat fraction of DECT with MMD and the histologic fat fraction showed a mean difference of -3.0%, which indicated good agreement of the MMD fat fraction of DECT with histologic examination as a reference standard and MR fat quantification as a technical standard. The 95% Bland-Altman limits of agreement between the DECT using the MMD fat fraction and the pathologic fat fraction or MR IDEAL IQ fat fraction were -23.8% to

Figure 7. In the human study, Bland-Altman plots of the fat fractions (%) of MDCT with MMD and MR IDEAL (a), the fat fractions of MDCT with MMD and the pathology results, and the fat fractions of MR IDEAL and the pathology results (c). Note that the high accuracy of the MDCT MMD fat fraction for the quantitative estimation of hepatic steatosis, compared with histologic examination as the reference standard and MR fat quantification as the technical standard.

(a)

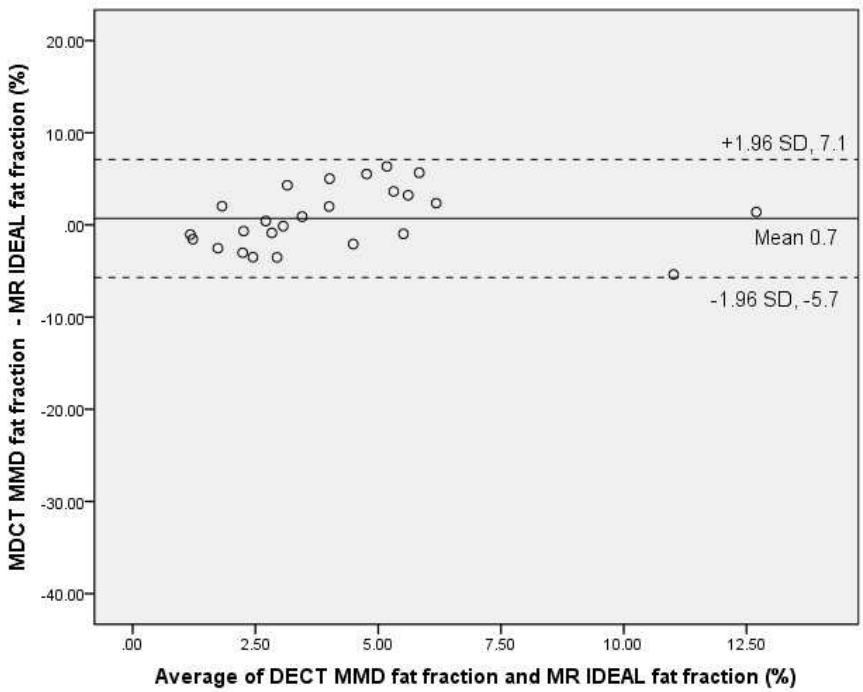

(b)

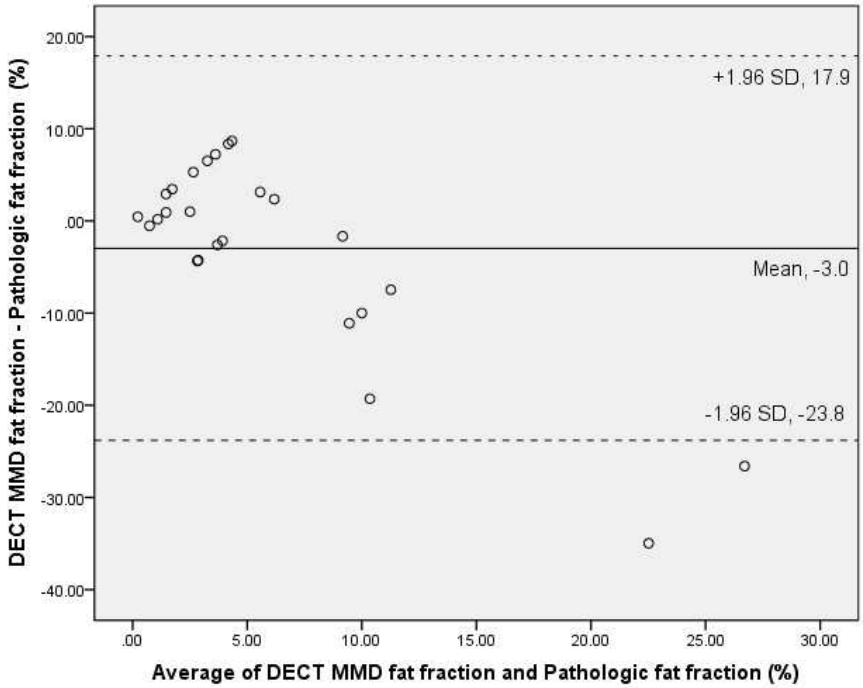
20.00
10.00
.00
-10.00
-20.00
-30.00
-40.00
+1.96 SD, 17.9
Mean, -3.0
-1.96 SD, -23.8
DECT MMD fat fraction - Pathologic fat fraction (%)
.00
5.00
10.00
15.00
20.00
25.00
30.00
Average of DECT MMD fat fraction and Pathologic fat fraction (%)

(c)

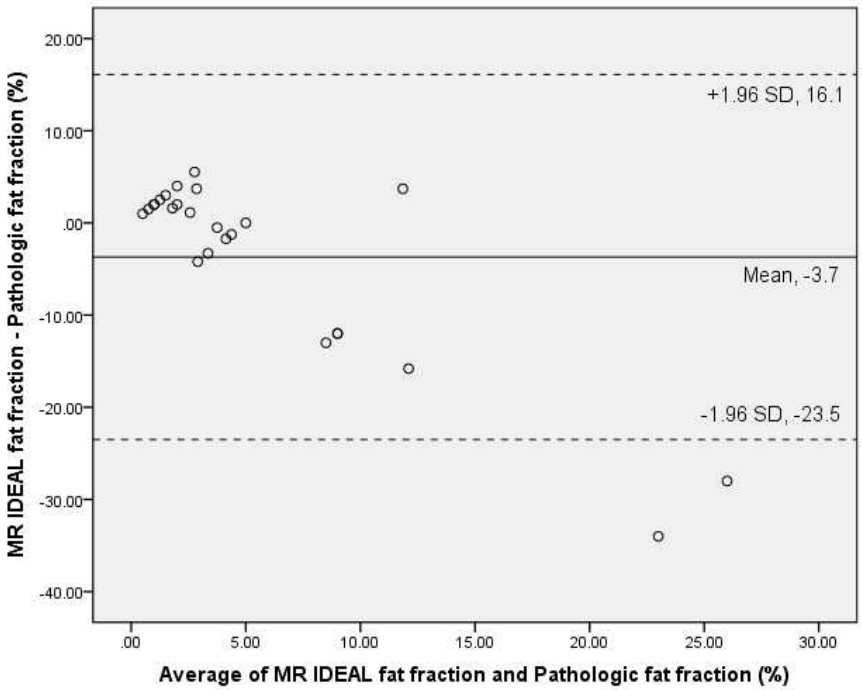
20.00
10.00
.00
-10.00
-20.00
-30.00
-40.00
+1.96 SD, 16.1
Mean, -3.7
-1.96 SD, -23.5
MR IDEAL fat fraction - Pathologic fat fraction (%)
.00
5.00
10.00
15.00
20.00
25.00
30.00
Average of MR IDEAL fat fraction and Pathologic fat fraction (%)

23.8% for the histologic examination and -5.7% to 7.1% for the MR IDEAL technique, and thus indicating the high accuracy of DECT using MMD for quantitatively estimating hepatic steatosis. Also, the Bland-Altman plot comparing the fat fraction of MR IDEAL IQ and that of histologic examination showed a mean difference of -3.7% with the 95% Bland-Altman limits of agreement of -23.5% to 16.1%, which does not differ from the Bland-Altman plot comparing the fat fraction of DECT using MMD and that of pathology. However, the mean difference of the Bland-Altman plot comparing the equation-based, estimated fat fraction of DECT with MMD and the histologic fat fraction, was 10.0% (not shown in Figure 7), which showed poorer agreement than did the measured fat fraction of DECT with MMD.

Diagnostic Performance of DECT with MMD for detection of hepatic steatosis

Table 3 shows the summary of the diagnostic performance and cutoff values of the ROC analysis in the human study. For detecting more than 5% hepatic steatosis, the cutoff values were set at 50.0 HU for the precontrast SECT, 3.5% for the fat fraction of DECT with MMD, and 4% for the fat fraction of MR IDEAL IQ. The sensitivities and specificities were 75% and 70.6% for the precontrast SECT, 87.5% and 64.7% for the fat fraction of DECT with MMD, and 62.5% and 88.2% for MR IDEAL, respectively. When the cutoff value for precontrast SECT to diagnose more than 10% hepatic steatosis was set at 44.7 HU, the sensitivity was 33.3% with 100% specificity.

The cutoff value for DECT with MMD was also 3.5% for detecting more than 10% hepatic steatosis with 83.3% sensitivity and 57.9% specificity. DECT with MMD showed a much higher sensitivity than SECT with lower specificity. Regarding the MR IDEAL IQ, when the cutoff value for diagnosis of more than 10% hepatic steatosis was set at 4%, the sensitivity was 66.7% and the specificity was 84.2%. Although the DECT with MMD provided higher sensitivity than MR IDEAL IQ and the MR IDEAL IQ showed higher specificity than DECT with MMD for detecting more than 5% or 10% hepatic steatosis, there was no statistical difference of the area under the ROC curves between the methods ($P = 0.749$ for $\geq$ 5% steatosis, $P = 0.220$ for $\geq$ 10% steatosis).

Table 3. Summary of the diagnostic performance and cutoff values of the CT number of SECT, and the fat fractions of DECT with MMD and MR IDEAL for detecting more than 5% or 10% hepatic steatosis, in the human study.

	Modality	AUROC	Criterion	Sensitivity	Specificity
≥5% hepatic steatosis	**SECT**	0.706 (0.491 - 0.869)	50.0	75.0%	70.6%
	DECT with MMD	0.721 (0.507 - 0.880)	3.5	87.5%	64.7%
	MR IDEAL	0.772 (0.562 - 0.914)	4	62.5%	88.2%
≥10% hepatic steatosis	**SECT**	0.632 (0.417 - 0.814)	44.7	33.3%	100%
	DECT with MMD	0.632 (0.417 - 0.814)	3.5	83.3%	57.9%
	MR IDEAL	0.816 (0.611 - 0.941)	4	66.7%	84.2%

Note – Number in parentheses are the 95% confidence interval values; SECT = single-energy CT, DECT = dual-energy CT, MMD = multi-material decomposition, IDEAL = iterative decomposition of water and fat using echo-asymmetry and the least-squares estimation quantitative sequence, AUROC: area under the ROC curve

DISCUSSION

The animal study results demonstrated that the HFFs of DECT with MMD were well-correlated with those of pathology and MRI, and provided consistent fat-fraction results even in the presence of iodinated contrast media. However, in the human study, HFF of DECT with MMD showed good agreement with the MRI and pathology results. The ROC analysis in the animal study also showed DECT with MMD to have comparable diagnostic performance with that of the precontrast SECT and MRI, for detecting more than 5% hepatic steatosis. In this human study, DECT with MMD showed relatively higher sensitivity and lower specificity than did precontrast SECT and MRI, however, the overall diagnostic performance was similar between the methods.

Until now, there have been controversial reports regarding the value of DECT for hepatic fat quantification. Some previous reports have suggested that DECT have showed promise for the identification of various soft-tissue types, calcified structures, and iodinated contrast media (42, 43), and that DECT was able to accurately predict the liver fat content in an animal study (25). The value of DECT for fat quantification could be attributed to the fact that the DECT data permits distinguishing materials with comparable atomic numbers due to differences in the photoelectric effect and Compton scatter on CT attenuation at different photon energies (35, 44-46). However, other reports maintain that dual-energy images generated using different ratios of the 80kVp and 140kVp data were not helpful for detecting fatty infiltration of

the liver in the presence of hemochromatosis or hemosiderosis (26, 32, 47). Based on this animal study results which demonstrated that the quantification of HFF using DECT with MMD is strongly correlated with the histologic fat fraction even in the presence of iodinated contrast media, it is expected that the precontrast scan would be omitted in some patients so that the radiation dose from CT scanning, which has become one of the major recent concerns, could be decreased.

In the present study, the hepatic attenuation coefficients on precontrast SECT or DECT showed a negative correlation with the pathologic HFF. However, although the degree of hepatic steatosis can be estimated by measuring the hepatic attenuation coefficient (22, 24, 48, 49), there are some limitations in the quantification of HFF using SECT. First, there were different CT attenuation values when CT scanning was performed at different energy levels in the same liver (49). The CT attenuation value was changed according to the influence of equipment, scanning qualification, etc. (25, 32). However, the tendency toward a negative linear correlation between the CT attenuation value and the histologic fat fraction was assured in this study. In addition, in the presence of iron or iodinated contrast media, quantification of HFF is not possible with SECT (48). Both iron and iodinated contrast media confound measurements by an increase in attenuation with higher iron or iodine concentrations, i.e. an inverse effect to fat (32, 50). This problem is one of the clinical issues because iron sometimes co-exists with fat infiltration in chronic liver disease. Moreover, quantification of HFF is also desirable in contrast-enhanced CT studies of the liver. Further study is warranted to

determine whether DECT with MMD could demonstrate an acceptable range of diagnostic accuracy for estimating HFF in the presence of both hepatic iron deposition and hepatic steatosis.

Interestingly, in the animal experiment, although the HFF values of DECT with MMD were well-correlated with the histologic fat fraction, the absolute values of the fat fraction from DECT and pathology differed and showed poor agreement. The histologic fat fraction in the animal experiment was approximately three to four times larger than that of DECT with MMD (P = 0.001). On the other hand, the human study results showed that the value of hepatic fat quantification of DECT with MMD has good agreement with that of histologic examination as a reference standard and that of MRI as a technical standard. For that reason, the equation regarding the HFF values of the MMD of precontrast DECT and the pathology results, both of which were obtained in the animal study, did not work in the human study. This difference would be due to the difference of the evaluation method and the protocol, and above all, the fat accumulation pattern in the rabbit liver which was mainly microvesicular hepatic steatosis rather than the macrovesicular pattern usually observed in human hepatic steatosis. Considering that the fat fractions of DECT with MMD and MR IDEAL IQ did not differ significantly (P = 0.061 - 0.266) in the animal experiment, the imaging modalities, such as CT and MRI, might not completely reflect the microvesicular steatosis on the fat-fraction map. Actually, considering some previous studies (51-54) which reported that the visual histologic fat fraction was two or three times higher than the fat fraction values obtained from CT, dual-gradient-echo MRI, and even MRS, it

is encouraging that the mean differences of Bland-Altman plots comparing the fat fractions of DECT with MMD, MR IDEAL, and the pathology results did not differ significantly from zero in this human study.

The LFQ algorithm used in this study uses fat, liver tissue, and blood in the material basis and also considers iodinated contrast media by applying the VUE image in the case of post-contrast DECT images. However, regarding the fat fraction of post-contrast DECT with MD in this animal study, rather than MMD, the results were negative values, and which is impossible in the real world. This is the limitation of the MD which considers only two material bases of fat and soft tissue. Actually, the composition of human organs and tissues is too complex for two-material decomposition to make an accurate material-specific image with only two materials in the material basis. It is said that addressing this problem was the motivation for the development of the MMD (37-39).

This study has some limitations. First, the numbers of study subjects in the hepatic steatosis severity groups and the control group were relatively small. In addition, the moderate degree of hepatic steatosis was not well-established in this animal experiment, and there was also only two moderate degrees of hepatic steatosis and no severe degree of hepatic steatosis in this human study. Next, the iron overloaded animal model with hepatic steatosis was not used for the accuracy evaluation of DECT with MMD in the quantification of HFF. There may be some methods to create an iron overload in animal experiments, such as a high iron diet for several to 12 months (55-57), intravenous or intramuscular injection of iron dextran or iron sorbitol for several months (58,

59), or injection of an iron oxide MR contrast agent or intravenous iron supplement at the time of the imaging study. However, these methods were not feasible in this study. Last, this human study did not evaluate the accuracy of DECT with MMD in the situation of the presence of iron or iodinated contrast media and did not record the presence of the iron on the pathologic results. Therefore, further studies are needed to assess the accuracy of DECT with MMD in HFF quantification in the presence of iron.

In conclusion, the quantification of HFF using DECT with MMD is well-correlated and shows good agreement with the histologic and MRI fat fractions even in the presence of iodinated contrast media and they have comparable sensitivity and specificity to the histology and MRI.

Acknowledgements

This study was supported by GE Healthcare CT research.

REFERENCES

1. McCullough AJ. Update on nonalcoholic fatty liver disease. Journal of clinical gastroenterology. 2002;34(3):255-62. Epub 2002/03/02.

2. Regimbeau JM, Colombat M, Mognol P, Durand F, Abdalla E, Degott C, et al. Obesity and diabetes as a risk factor for hepatocellular carcinoma. Liver transplantation : official publication of the American Association for the Study of Liver Diseases and the International Liver Transplantation Society. 2004;10(2 Suppl 1):S69-73. Epub 2004/02/06.

3. Bugianesi E, Leone N, Vanni E, Marchesini G, Brunello F, Carucci P, et al. Expanding the natural history of nonalcoholic steatohepatitis: from cryptogenic cirrhosis to hepatocellular carcinoma. Gastroenterology. 2002;123(1):134-40. Epub 2002/07/10.

4. Kooby DA, Fong Y, Suriawinata A, Gonen M, Allen PJ, Klimstra DS, et al. Impact of steatosis on perioperative outcome following hepatic resection. Journal of gastrointestinal surgery : official journal of the Society for Surgery of the Alimentary Tract. 2003;7(8):1034-44. Epub 2003/12/17.

5. Belghiti J, Hiramatsu K, Benoist S, Massault P, Sauvanet A, Farges O. Seven hundred forty-seven hepatectomies in the 1990s: an update to evaluate the actual risk of liver resection. Journal of the American College of Surgeons. 2000;191(1):38-46. Epub 2000/07/18.

6. Behrns KE, Tsiotos GG, DeSouza NF, Krishna MK, Ludwig J, Nagorney DM. Hepatic steatosis as a potential risk factor for major hepatic resection. Journal of gastrointestinal surgery : official journal of the Society

for Surgery of the Alimentary Tract. 1998;2(3):292-8. Epub 1998/12/08.

7. Tsang LL, Chen CL, Huang TL, Chen TY, Wang CC, Ou HY, et al. Preoperative imaging evaluation of potential living liver donors: reasons for exclusion from donation in adult living donor liver transplantation. Transplantation proceedings. 2008;40(8):2460-2. Epub 2008/10/22.

8. Park SH, Kim PN, Kim KW, Lee SW, Yoon SE, Park SW, et al. Macrovesicular hepatic steatosis in living liver donors: use of CT for quantitative and qualitative assessment. Radiology. 2006;239(1):105-12. Epub 2006/02/18.

9. Kim SH, Lee JM, Kim JH, Kim KG, Han JK, Lee KH, et al. Appropriateness of a donor liver with respect to macrosteatosis: application of artificial neural networks to US images--initial experience. Radiology. 2005;234(3):793-803. Epub 2005/01/25.

10. Ploeg RJ, D'Alessandro AM, Knechtle SJ, Stegall MD, Pirsch JD, Hoffmann RM, et al. Risk factors for primary dysfunction after liver transplantation--a multivariate analysis. Transplantation. 1993;55(4):807-13.

11. Ratziu V, Charlotte F, Heurtier A, Gombert S, Giral P, Bruckert E, et al. Sampling variability of liver biopsy in nonalcoholic fatty liver disease. Gastroenterology. 2005;128(7):1898-906. Epub 2005/06/09.

12. Yokoo T, Bydder M, Hamilton G, Middleton MS, Gamst AC, Wolfson T, et al. Nonalcoholic fatty liver disease: diagnostic and fat-grading accuracy of low-flip-angle multiecho gradient-recalled-echo MR imaging at 1.5 T. Radiology. 2009;251(1):67-76. Epub 2009/02/18.

13. Smith EH. Complications of percutaneous abdominal fine-needle

biopsy. Review. Radiology. 1991;178(1):253-8. Epub 1991/01/01.

14. Saadeh S, Younossi ZM, Remer EM, Gramlich T, Ong JP, Hurley M, et al. The utility of radiological imaging in nonalcoholic fatty liver disease. Gastroenterology. 2002;123(3):745-50. Epub 2002/08/29.

15. Strauss S, Gavish E, Gottlieb P, Katsnelson L. Interobserver and intraobserver variability in the sonographic assessment of fatty liver. AJR American journal of roentgenology. 2007;189(6):W320-3. Epub 2007/11/22.

16. Graif M, Yanuka M, Baraz M, Blank A, Moshkovitz M, Kessler A, et al. Quantitative estimation of attenuation in ultrasound video images: correlation with histology in diffuse liver disease. Investigative radiology. 2000;35(5):319-24. Epub 2000/05/10.

17. Levenson H, Greensite F, Hoefs J, Friloux L, Applegate G, Silva E, et al. Fatty infiltration of the liver: quantification with phase-contrast MR imaging at 1.5 T vs biopsy. AJR American journal of roentgenology. 1991;156(2):307-12. Epub 1991/02/01.

18. Qayyum A, Goh JS, Kakar S, Yeh BM, Merriman RB, Coakley FV. Accuracy of liver fat quantification at MR imaging: comparison of out-of-phase gradient-echo and fat-saturated fast spin-echo techniques--initial experience. Radiology. 2005;237(2):507-11. Epub 2005/10/26.

19. Joe E, Lee JM, Kim KW, Lee KB, Kim SJ, Baek JH, et al. Quantification of hepatic macrosteatosis in living, related liver donors using T1-independent, T2*-corrected chemical shift MRI. Journal of magnetic resonance imaging : JMRI. 2012;36(5):1124-30. Epub 2012/07/05.

20. Clark JM, Brancati FL, Diehl AM. Nonalcoholic fatty liver disease.

Gastroenterology. 2002;122(6):1649-57. Epub 2002/05/23.

21. Johnston RJ, Stamm ER, Lewin JM, Hendrick RE, Archer PG. Diagnosis of fatty infiltration of the liver on contrast enhanced CT: limitations of liver-minus-spleen attenuation difference measurements. Abdominal imaging. 1998;23(4):409-15. Epub 1998/07/15.

22. Ricci C, Longo R, Gioulis E, Bosco M, Pollesello P, Masutti F, et al. Noninvasive in vivo quantitative assessment of fat content in human liver. Journal of hepatology. 1997;27(1):108-13. Epub 1997/07/01.

23. Kammen BF, Pacharn P, Thoeni RF, Lu Y, Qayyum A, Coakly F, et al. Focal fatty infiltration of the liver: analysis of prevalence and CT findings in children and young adults. AJR American journal of roentgenology. 2001;177(5):1035-9. Epub 2001/10/20.

24. Kawata R, Sakata K, Kunieda T, Saji S, Doi H, Nozawa Y. Quantitative evaluation of fatty liver by computed tomography in rabbits. AJR American journal of roentgenology. 1984;142(4):741-6. Epub 1984/04/01.

25. Wang B, Gao Z, Zou Q, Li L. Quantitative diagnosis of fatty liver with dual-energy CT. An experimental study in rabbits. Acta radiologica. 2003;44(1):92-7.

26. Lee SW, Park SH, Kim KW, Choi EK, Shin YM, Kim PN, et al. Unenhanced CT for assessment of macrovesicular hepatic steatosis in living liver donors: comparison of visual grading with liver attenuation index. Radiology. 2007;244(2):479-85. Epub 2007/07/21.

27. Panicek DM, Giess CS, Schwartz LH. Qualitative assessment of liver for fatty infiltration on contrast-enhanced CT: is muscle a better standard

of reference than spleen? Journal of computer assisted tomography. 1997;21(5):699-705. Epub 1997/09/19.

28. Limanond P, Raman SS, Lassman C, Sayre J, Ghobrial RM, Busuttil RW, et al. Macrovesicular hepatic steatosis in living related liver donors: correlation between CT and histologic findings. Radiology. 2004;230(1):276-80.

29. Thomsen C, Becker U, Winkler K, Christoffersen P, Jensen M, Henriksen O. Quantification of liver fat using magnetic resonance spectroscopy. Magnetic resonance imaging. 1994;12(3):487-95. Epub 1994/01/01.

30. Tang A, Tan J, Sun M, Hamilton G, Bydder M, Wolfson T, et al. Nonalcoholic fatty liver disease: MR imaging of liver proton density fat fraction to assess hepatic steatosis. Radiology. 2013;267(2):422-31. Epub 2013/02/06.

31. Hines CD, Frydrychowicz A, Hamilton G, Tudorascu DL, Vigen KK, Yu H, et al. T(1) independent, T(2) (*) corrected chemical shift based fat-water separation with multi-peak fat spectral modeling is an accurate and precise measure of hepatic steatosis. Journal of magnetic resonance imaging : JMRI. 2011;33(4):873-81. Epub 2011/03/31.

32. Raptopoulos V, Karellas A, Bernstein J, Reale FR, Constantinou C, Zawacki JK. Value of dual-energy CT in differentiating focal fatty infiltration of the liver from low-density masses. AJR American journal of roentgenology. 1991;157(4):721-5. Epub 1991/10/01.

33. Mendler MH, Bouillet P, Le Sidaner A, Lavoine E, Labrousse F,

Sautereau D, et al. Dual-energy CT in the diagnosis and quantification of fatty liver: limited clinical value in comparison to ultrasound scan and single-energy CT, with special reference to iron overload. Journal of hepatology. 1998;28(5):785-94. Epub 1998/06/13.

34. Goldberg HI, Cann CE, Moss AA, Ohto M, Brito A, Federle M. Noninvasive quantitation of liver iron in dogs with hemochromatosis using dual-energy CT scanning. Investigative radiology. 1982;17(4):375-80. Epub 1982/07/01.

35. Liu X, Yu L, Primak AN, McCollough CH. Quantitative imaging of element composition and mass fraction using dual-energy CT: three-material decomposition. Medical physics. 2009;36(5):1602-9. Epub 2009/06/24.

36. Fu JF, Fang YL, Liang L, Wang CL, Hong F, Dong GP. A rabbit model of pediatric nonalcoholic steatohepatitis: the role of adiponectin. World journal of gastroenterology : WJG. 2009;15(8):912-8. Epub 2009/02/28.

37. Mendonca P, Lamb P, Sahani D. A Flexible Method for Multi-Material Decomposition of Dual-Energy CT Images. IEEE transactions on medical imaging. 2013. Epub 2013/09/24.

38. Andras Kristona PM, Alvin Silva, Robert G. Paden, William Pavlicek, Dushyant Sahani, Benedek Janos Kis, Laszlo Rusko, Darin Okerlund, and Rahul Bhotika. Liver fat quantification using fast kVp-switching dual energy CT. SPIE Medical Imaging International Society for Optics and Photonics. 2011.

39. Fischer MA, Gnannt R, Raptis D, Reiner CS, Clavien PA, Schmidt B, et al. Quantification of liver fat in the presence of iron and iodine: an ex-vivo

dual-energy CT study. Investigative radiology. 2011;46(6):351-8. Epub 2011/01/26.

40. Yushkevich PA, Piven J, Hazlett HC, Smith RG, Ho S, Gee JC, et al. User-guided 3D active contour segmentation of anatomical structures: significantly improved efficiency and reliability. NeuroImage. 2006;31(3):1116-28. Epub 2006/03/21.

41. Kleiner DE, Brunt EM, Van Natta M, Behling C, Contos MJ, Cummings OW, et al. Design and validation of a histological scoring system for nonalcoholic fatty liver disease. Hepatology. 2005;41(6):1313-21.

42. Zachrisson H, Engstrom E, Engvall J, Wigstrom L, Smedby O, Persson A. Soft tissue discrimination ex vivo by dual energy computed tomography. European journal of radiology. 2010;75(2):e124-8. Epub 2010/03/12.

43. Robinson E, Babb J, Chandarana H, Macari M. Dual source dual energy MDCT: comparison of 80 kVp and weighted average 120 kVp data for conspicuity of hypo-vascular liver metastases. Investigative radiology. 2010;45(7):413-8. Epub 2010/05/12.

44. Coursey CA, Nelson RC, Boll DT, Paulson EK, Ho LM, Neville AM, et al. Dual-energy multidetector CT: how does it work, what can it tell us, and when can we use it in abdominopelvic imaging? Radiographics : a review publication of the Radiological Society of North America, Inc. 2010;30(4):1037-55. Epub 2010/07/16.

45. Graser A, Becker CR, Staehler M, Clevert DA, Macari M, Arndt N, et al. Single-phase dual-energy CT allows for characterization of renal masses

as benign or malignant. Investigative radiology. 2010;45(7):399-405. Epub 2010/05/26.

46. Yeh BM, Shepherd JA, Wang ZJ, Teh HS, Hartman RP, Prevrhal S. Dual-energy and low-kVp CT in the abdomen. AJR American journal of roentgenology. 2009;193(1):47-54. Epub 2009/06/23.

47. Oelckers S, Graeff W. In situ measurement of iron overload in liver tissue by dual-energy methods. Physics in medicine and biology. 1996;41(7):1149-65. Epub 1996/07/01.

48. Boll DT, Merkle EM. Diffuse liver disease: strategies for hepatic CT and MR imaging. Radiographics : a review publication of the Radiological Society of North America, Inc. 2009;29(6):1591-614. Epub 2009/12/05.

49. Ma X, Holalkere NS, Kambadakone RA, Mino-Kenudson M, Hahn PF, Sahani DV. Imaging-based quantification of hepatic fat: methods and clinical applications. Radiographics : a review publication of the Radiological Society of North America, Inc. 2009;29(5):1253-77. Epub 2009/09/17.

50. Hamer OW, Aguirre DA, Casola G, Lavine JE, Woenckhaus M, Sirlin CB. Fatty liver: imaging patterns and pitfalls. Radiographics : a review publication of the Radiological Society of North America, Inc. 2006;26(6):1637-53. Epub 2006/11/15.

51. d'Assignies G, Ruel M, Khiat A, Lepanto L, Chagnon M, Kauffmann C, et al. Noninvasive quantitation of human liver steatosis using magnetic resonance and bioassay methods. European radiology. 2009;19(8):2033-40. Epub 2009/03/13.

52. Marsman H, Matsushita T, Dierkhising R, Kremers W, Rosen C,

Burgart L, et al. Assessment of donor liver steatosis: pathologist or automated software? Human pathology. 2004;35(4):430-5. Epub 2004/04/30.

53. Cotler SJ, Guzman G, Layden-Almer J, Mazzone T, Layden TJ, Zhou XJ. Measurement of liver fat content using selective saturation at 3.0 T. Journal of magnetic resonance imaging : JMRI. 2007;25(4):743-8. Epub 2007/03/10.

54. Lee SS, Park SH, Kim HJ, Kim SY, Kim MY, Kim DY, et al. Non-invasive assessment of hepatic steatosis: prospective comparison of the accuracy of imaging examinations. Journal of hepatology. 2010;52(4):579-85. Epub 2010/02/27.

55. Stal P, Hultcrantz R. Iron increases ethanol toxicity in rat liver. Journal of hepatology. 1993;17(1):108-15. Epub 1993/01/01.

56. Asare GA, Kew MC, Mossanda KS, Paterson AC, Siziba K, Kahler-Venter CP. Effects of exogenous antioxidants on dietary iron overload. Journal of clinical biochemistry and nutrition. 2009;44(1):85-94. Epub 2009/01/30.

57. Valerio LG, Jr., Petersen DR. Characterization of hepatic iron overload following dietary administration of dicyclopentadienyl iron (Ferrocene) to mice: cellular, biochemical, and molecular aspects. Experimental and molecular pathology. 2000;68(1):1-12. Epub 2000/01/21.

58. Turbino-Ribeiro SM, Silva ME, Chianca DA, Jr., De Paula H, Cardoso LM, Colombari E, et al. Iron overload in hypercholesterolemic rats affects iron homeostasis and serum lipids but not blood pressure. The Journal of nutrition. 2003;133(1):15-20. Epub 2003/01/07.

59. Kudo H, Suzuki S, Watanabe A, Kikuchi H, Sassa S, Sakamoto S.

Effects of colloidal iron overload on renal and hepatic siderosis and the femur in male rats. Toxicology. 2008;246(2-3):143-7. Epub 2008/02/22.

국문 초록

서론: 이중에너지 전산화 단층촬영 (DECT)과 다물질 분해 방법 (MMD)을 이용한 간 내 지방분율 정량화에 있어, 조직학적 결과 및 자기공명영상을 표준으로 삼아 그 정확성과 실현 가능성을 평가하며, 조영전 전산화 단층촬영과 비교한 진단능을 평가하고자 한다.

방법: 본 연구는 소속 기관의 동물실험윤리위원회와 연구윤리심의위원회의 승인을 받았다. 동물연구를 위해 16 마리의 토끼를 4 군으로 나누고, 고지방, 고콜레스테롤 사료를 각각 0, 2, 4, 6 주 동안 식이시켜 다양한 정도의 지방간을 유발시켰다. 6 주 경과 후에 조영전 단일에너지 전산화 단층촬영(SECT)과 다중촬영 DECT 를 시행하고, MMD 를 이용하여 DECT 자료에서부터 간 지방분율 영상을 얻었다. 같은 날 화학이동 자기공명영상(MRI)과 간 조직학적 검사를 시행하였다. MRI 와 조직학적 검사를 통하여 간의 지방분율을 측정하였다. 사람연구를 위해 14 명의 생체간이식 공여자와 11 명의 간이식 수여자를 모집하였고, 이들은 조영전 DECT 와 MRI, 및 수술을 시행받았다. CT 감쇄 값을 CT 영상에서 측정하고, DECT 로부터 얻은 지방분율 영상과 MRI 에서 간의 지방분율을 측정하고, 간 조직 검체에서 조직학적 지방 축적 정도를 평가하였다. DECT 에서 얻은 간 지방분율과 MRI 및 조직학적으로 구한 간지방분율 사이의

상관관계및 일치도를 분석하고, 진단능으로 민감도와 특이도를 평가하였다

결과: 조직학적 간 지방분율은 조영전 영상의 CT 감쇄 값과는 강한 음의 선형 상관관계를 보였다. 동물연구에서, DECT 에서 얻은 간 지방분율은 MRI 및 조직학적으로 구한 간지방분율과 강한 상관관계를 보였으며, 요오드를 함유하고 있는 조영제가 있음에도 불구하고 다중촬영 DECT 에서 얻은 간지방분율 값에는 큰 차이가 없었다. 하지만 DECT 에서 얻은 간 지방분율 값과 MRI 및 조직학적으로 구한 간지방분율 값의 일치도는 좋지 않았다. 사람연구에서는, 비록 DECT 에서 얻은 간 지방분율 값과 MRI 및 조직학적으로 구한 간 지방분율 값 사이에 상관관계는 없었으나, 그 값들 사이에 높은 일치도를 나타내었다. DECT 의 간 지방분율 진단에 대한 민감도와 특이도는 조영전 전산화 단층촬영 및 자기공명영상의 결과와 비견할 만하였다 (P = 0.17–0.82).

결론: 이중에너지 전산화 단층촬영과 다물질 분해 방법을 이용한 간내 지방분율 정량화는 요오드를 함유한 조영제가 있는 경우에도 조직학적 및 자기공명영상의 간 지방분율과 강한 상관관계와 높은 일치도를 보이며, 조영전 전산화 단층촬영과 자기공명영상과 비교할만한 민감도와 특이도를 보인다.

주요어 : 이중에너지 전산화 단층촬영; 다물질 분해 방법; 간 내 지방분율 정량화; 토끼 지방간

학번 : 2012-21725